

# 1,3-Diradicals Embedded in Curved Paraphenylenes Units: Singlet versus Triplet State and In-Plane Aromaticity

Yuki Miyazawa, Zhe Wang, Misaki Matsumoto, Sayaka Hatano, Ivana Antol,\* Eiichi Kayahara, Shigeru Yamago,\* and Manabu Abe\*



Cite This: *J. Am. Chem. Soc.* 2021, 143, 7426–7439



Read Online

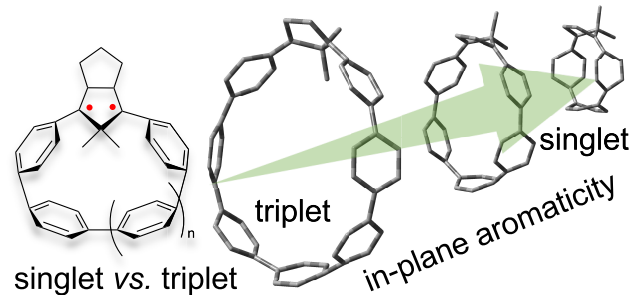
ACCESS |

Metrics & More

Article Recommendations

Supporting Information

**ABSTRACT:** Curved  $\pi$ -conjugated molecules and open-shell structures have attracted much attention from the perspective of fundamental chemistry, as well as materials science. In this study, the chemistry of 1,3-diradicals (DRs) embedded in curved cycloparaphenylenes (CPPs) structures, DR-( $n+3$ )CPPs ( $n = 0–5$ ), was investigated to understand the effects of the curvature and system size on the spin–spin interactions and singlet versus triplet state, as well as their unique characteristics such as in-plane aromaticity. A triplet ground state was predicted for the larger 1,3-diradicals, such as the seven- and eight-paraphenylen-unit-containing diradicals DR-7CPP ( $n = 4$ ) and DR-8CPP ( $n = 5$ ), by quantum chemical calculations. The smaller-sized diradicals DR-( $n+3$ )CPPs ( $n = 0–3$ ) were found to possess singlet ground states. Thus, the ground-state spin multiplicity is controlled by the size of the paraphenylen cycle. The size effect on the ground-state spin multiplicity was confirmed by the experimental generation of DR-6CPP in the photochemical denitrogenation of its azo-containing precursor (AZ-6CPP). Intriguingly, a unique type of in-plane aromaticity emerged in the smaller-sized singlet states such as S-DR-4CPP ( $n = 1$ ), as proven by nucleus-independent chemical shift calculations (NICS) and an analysis of the anisotropy of the induced current density (ACID), which demonstrate that homoconjugation between the 1,3-diradical moiety arises because of the curved and distorted bonding system.



## INTRODUCTION

In the past decade, open-shell molecules have attracted considerable attention not only in the field of reactive intermediates but also in materials science. For example, radical-based light-emitting diodes have been developed using isolatable triaryl methyl radicals,<sup>1–3</sup> magnetically robust high-spin molecules have been developed using new molecular designs,<sup>4,5</sup> and a new bonding system,  $\pi$  single bonding, has emerged through research into localized diradicals.<sup>6–13</sup> Furthermore, the isolation of singlet diradicaloids such as Tchitchibabin derivatives has revealed their singlet fission behavior and nonlinear optical character, and these are now hot topics in  $\pi$ -conjugated materials.<sup>7,14–24</sup> To date, we have investigated the localized 1,3-diradicals DR (see Figure 1a), which are key intermediates in bond homolysis.<sup>25–29</sup> The ground-state spin multiplicity is typically controlled by the substituents at the C2 position, and the triplet ground state for DR having X = H, CH<sub>3</sub> can be switched to a singlet ground state by the introduction of electron-donating and electron-withdrawing substituents, for example, X = F, OR, SiR<sub>3</sub> (Figure 1a).<sup>12,30</sup>

In the late 2000s, pioneering studies in the synthesis of a new series of  $\pi$ -conjugated molecules, cycloparaphenylenes (CPPs), were reported; since then, these intriguing molecules

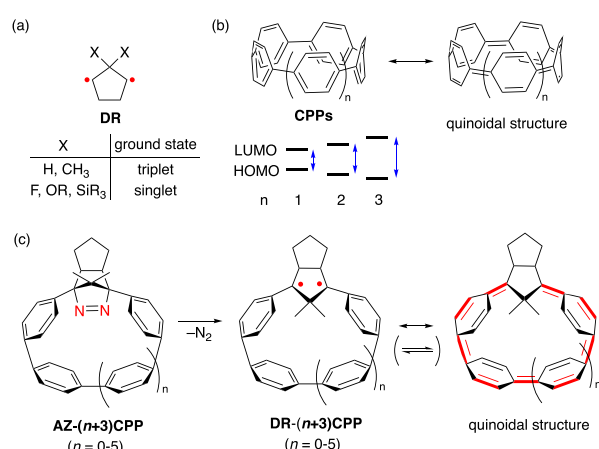


**Figure 1.** (a) Substituent effects on the ground-state spin multiplicity of cyclopentane-1,3-diyil diradicals. (b) Effect of size on the quinoidal character of cycloparaphenylenes. (c) This study.

Received: February 3, 2021

Published: April 26, 2021



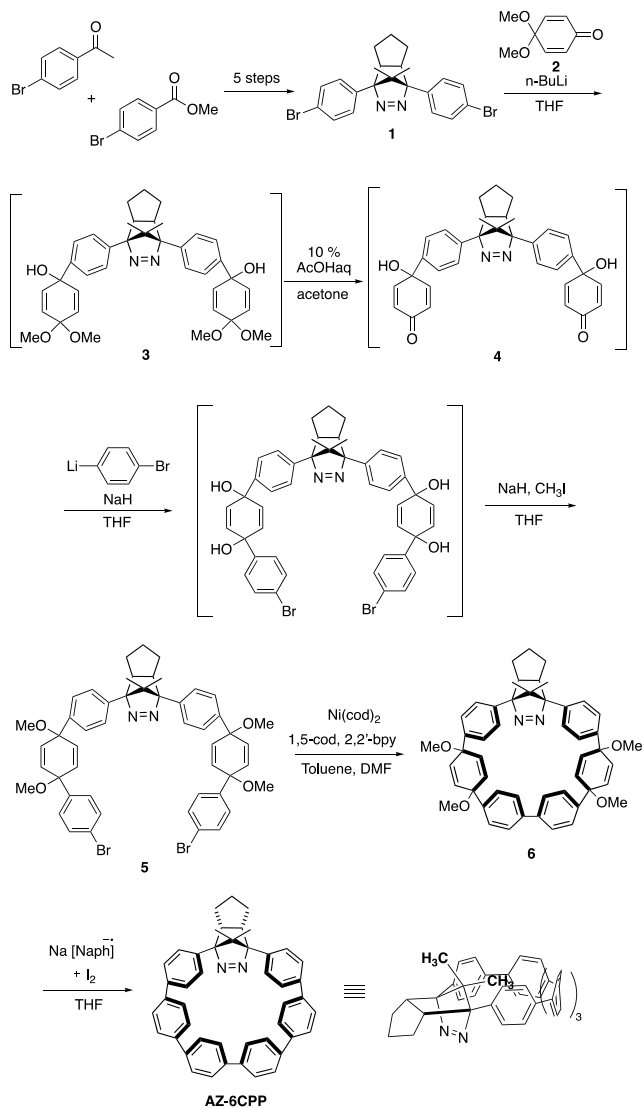
have attracted much attention.<sup>31–33</sup> The most striking feature of these hoop-shaped molecules is the hypsochromic shift of the HOMO–LUMO energy gap with an increasing number of benzene rings in the CPP structures (Figure 1b).<sup>34–36</sup> This behavior is totally opposite to that of linear paraphenlenes. This unique behavior is rationalized as being a result of the quinoidal contribution of the small CPPs arising from the diradical character induced by the curved structure of the benzene rings.<sup>37</sup> In the present study, we designed diradicals DR-(n+3)CPPs to investigate the quinoidal character in the hoop-shaped structures (Figure 1c). Among the precursors AZ-(n+3)CPPs featuring curved paraphenylene units, the novel azoalkane AZ-6CPP ( $n = 3$ ) was synthesized to investigate its electronic character and the corresponding chemistry of the diradical DR-6CPP ( $n = 3$ ). Furthermore, quantum chemical calculations were carried out for all diradicals DR-(n+3)CPP ( $n = 0–5$ ) to understand the experimental results for DR-6CPP and the effect of the ring size on the diradical chemistry in the hoop-shaped structure. In particular, we draw attention to the size effect on the ground-state spin multiplicity (singlet (S) versus triplet (T)) and interaction of the two spins with the curved  $\pi$ -electron system (quinoidal structure).

## RESULTS

**Synthesis of AZ-6CPP.** The synthetic route to AZ-6CPP is shown in Scheme 1. Double lithium bromide exchange of compound 1 and its addition to 4,4-dimethoxycyclohexane-2,5-dien-1-one (2) gave the diketal intermediate 3. Subsequent acid hydrolysis produced diketone 4.<sup>38</sup> The double arylation of 4 using (4-bromophenyl)lithium produced a diol, followed by dimethylation using NaH and MeI to afford dibromide 5 in 13% yield (four steps). The Yamamoto coupling of the dibromide followed by the reductive aromatization<sup>31</sup> of 6 afforded AZ-6CPP in approximately 1% total yield on the basis of the starting material. Single crystals were obtained by the gradual evaporation of a mixture of CHCl<sub>3</sub> and MeOH, and the strained structure was confirmed by an X-ray crystallographic analysis (Figure 2a). Two AZ-6CPP molecules were found in a single crystal lattice, and in this structure, a molecule of CHCl<sub>3</sub> occupies the curved paraphenylene unit. In the <sup>1</sup>H NMR spectrum (*vide infra*), the two CH<sub>3</sub> groups appeared at  $\delta$  –2.36 and –0.49 ppm relative to the signal of benzene ( $\delta$  7.16 ppm). The high-field resonance is a result of the aromatic ring current induced by the benzene rings in the macrocyclic structure. The dimethyl group was found to be *trans*-configured relative to the cyclopentane ring. The bond lengths, average torsion angles ( $\theta = 17.2^\circ$ ), and bending of the benzene rings ( $\alpha = 17.7^\circ$ ) of the paraphenylene units of AZ-6CPP were compared with those of *p*-sexiphenyl, the linear paraphenylene C<sub>6</sub>H<sub>5</sub>–(C<sub>6</sub>H<sub>4</sub>)<sub>4</sub>–C<sub>6</sub>H<sub>5</sub> (Figure 2b). Density functional theory (DFT) calculations at the B3LYP/6-31G(d) level of theory reproduced the molecular structure of AZ-6CPP well, although the torsion angles between the two benzene rings were computed to be slightly larger than those obtained in the X-ray analysis. The average torsion angle of curved AZ-6CPP ( $\alpha = 17.7^\circ$ ) was found to be approximately half of that of *p*-sexiphenyl.

**Absorption and Emission Spectroscopy Analysis of AZ-6CPP.** The absorption and emission spectra of AZ-6CPP are shown in Figure 3. A broad absorption at approximately 400 nm ( $\lambda_{\text{max}} = 404 \text{ nm}$ ,  $\epsilon = 7916 \text{ M}^{-1} \text{ cm}^{-1}$ ) and a structured band at about 330 nm ( $\lambda_{\text{max}} = 331 \text{ nm}$ ,  $\epsilon = 40509 \text{ M}^{-1} \text{ cm}^{-1}$ )

**Scheme 1. Synthesis of AZ-6CPP<sup>a</sup>**



<sup>a</sup>Abbreviations: THF, tetrahydrofuran; cod, cyclooctadiene; DMF, dimethylformamide; bpy, bipyridine; Naph, naphthalene.

were observed in the UV–vis absorption spectra (Figure 3a). The weak n– $\pi^*$  transition ( $\epsilon \approx 100 \text{ M}^{-1} \text{ cm}^{-1}$ ) of the azo chromophore (–N=N–) at approximately 360 nm seems to be hidden behind the strong absorption band from the  $\pi$ -conjugated system. Time-dependent (TD) DFT<sup>39</sup> calculations at the B3LYP/6-31G(d)<sup>40,41</sup> level of theory revealed that the absorption at around 400 nm can be attributed to the HOMO–LUMO transition, S<sub>0</sub> → S<sub>1</sub> ( $\lambda_{\text{calc}} = 431.7 \text{ nm}$ , Figure 3b,g), having an oscillator strength ( $f$ ) of 0.1748. The corresponding HOMO–LUMO transition (S<sub>0</sub> → S<sub>1</sub>) in the six-membered CPP ([6]CPP) is reported to be symmetry forbidden because the HOMO and LUMO conserve symmetry (Laporte forbidden).<sup>42–44</sup> A strong S<sub>0</sub> → S<sub>5</sub> absorption band, which mainly corresponds to the HOMO-1–LUMO (0.44) and HOMO–LUMO+2 (0.53) transitions, was computed with  $f = 1.0250$  at  $\lambda_{\text{calc}} = 327.1 \text{ nm}$  (Figure 3c,g), as found at approximately 320 nm in the experimental absorption spectrum (Figure 3a).

A structured fluorescence emission was observed in the spectra obtained under a nitrogen atmosphere; this emission,

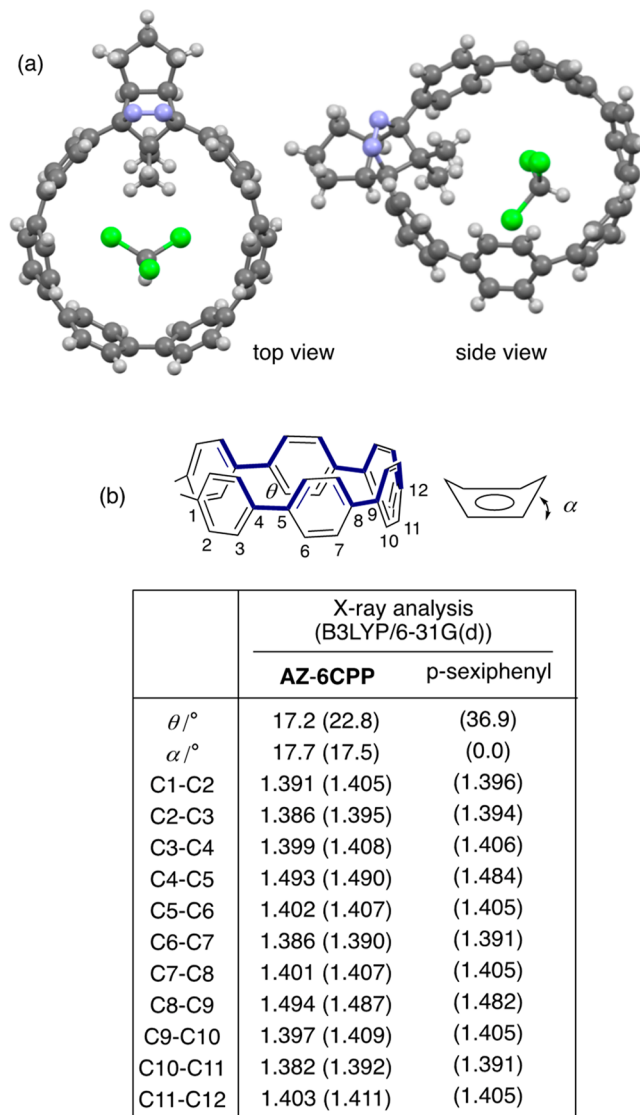
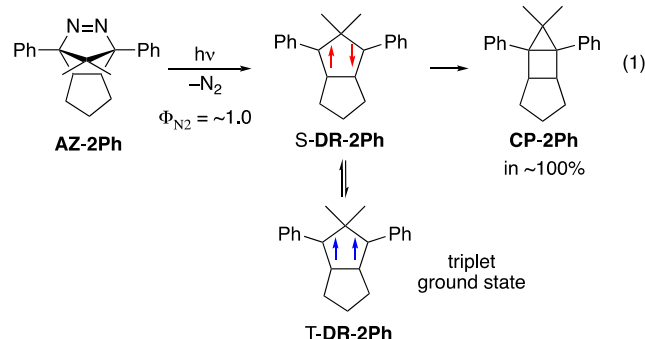


**Figure 2.** (a) X-ray structure of AZ-6CPP (black, carbon; gray, hydrogen; blue, nitrogen; green, chloride). (b) Experimentally and computationally determined (at the B3LYP/6-31G(d) level of theory in parentheses) torsion angles between the adjacent benzene-rings ( $\theta$ ) in deg, benzene bending angles ( $\alpha$  in deg), and bond lengths ( $\text{\AA}$ ) of the paraphenylene structures in AZ-6CPP and  $\text{C}_6\text{H}_5-(\text{CH}_2)_4-\text{C}_6\text{H}_5$  (*p*-sexiphenyl).

at approximately 500 nm ( $\lambda_{\text{onset}} = 433$  nm,  $\lambda = 475, 505$  nm), has a relatively high fluorescence quantum yield of 79% (Figure 3d) and, using this, the  $S_1$  state energy was estimated to be approximately 66 kcal mol<sup>-1</sup>. In contrast, the fluorescence quantum yields of small  $[n]$ CPPs ( $n = 5-8$ ) are reported to be less than 10%. Thus, the embedded azo moiety significantly changed the electronic transition and emission character of the curved  $\pi$ -conjugated molecule. A similar symmetry-breaking strategy to turn on HOMO–LUMO absorption and emission in small CPPs was reported by Jasti.<sup>45</sup> The lifetime of the fluorescence at 500 nm was determined to be  $\tau_f = 5.0$  ns under  $\text{N}_2$  at 295 K using the time-correlated single-photon-counting (TCSPC) method (Figure S76). Interestingly, the fluorescence quantum yield and lifetime decreased and were shortened by about 20% in air ( $[\text{O}_2] = 1.9$  mM) to 4.2 ns and 62%, respectively (Figure 3e and Figure S62), suggesting that the nonfluorescence process

was accelerated by molecular oxygen. Recently, Suenobu and Nakagawa reported<sup>46</sup> similar  $S_1$  state quenching by molecular oxygen for [9]-, [12]-, and [15]CPPs, thus generating triplet excited states of the CPP molecules. The phosphorescence of AZ-6CPP was not observed, even at 77 K, under a nitrogen atmosphere, which is behavior similar to that of small  $[n]$ CPPs ( $n = 5-7$ ). The triplet energy was computed to be 55.6 kcal mol<sup>-1</sup> at the UB3LYP/6-31G(d) level of theory. Thus, the energy difference with the  $S_1$  state,  $\Delta E_{ST} \approx 10$  kcal mol<sup>-1</sup>, is smaller than the singlet oxygen energy ( $^1\Delta_g = 22.5$  kcal mol<sup>-1</sup>). The generation of the  $T_1$  state of AZ-6CPP was expected in the  $S_1$  state quenching by  $^3\text{O}_2$  (see Figure 4d).<sup>47</sup>

**Transient Absorption Spectroscopy Analysis of AZ-6CPP.** Sub-nanosecond and sub-microsecond transient absorption (TA) measurements of AZ-6CPP ( $\text{Abs}_{355} = 1.0$ ) were conducted using randomly interleaved pulse train (RIPT)<sup>48</sup> and laser flash photolysis (LFP), respectively (Figure 4). Transient species were observed with absorption peaks at approximately 540, 600, and 660 nm in the sub-nanosecond TA analysis just after laser irradiation in argon-saturated benzene at 298 K. These transient species did not originate from the diradical generated by photochemical denitrogenation but from the  $\pi$ -conjugated paraphenylene moiety, because virtually no change in the UV–vis absorption spectra of the sample was observed before and after the TA measurements (Figures S56 and S57). This is reasonable because the molar extinction coefficient ( $\epsilon$ ) at 355 nm of the  $\pi-\pi^*$  excitation of AZ-6CPP is 7000 times larger than that of the  $n-\pi^*$   $\text{N}=\text{N}-$  chromophore of AZ-2Ph,  $\epsilon = 83 \text{ M}^{-1} \text{ cm}^{-1}$ , whose excitation is necessary for denitrogenation to give the diradical intermediate DR-2Ph having a triplet ground state. The quantitative formation of the ring-closed compound CP-2Ph via the photochemical denitrogenation of AZ-2Ph has been reported with a high quantum yield of  $\Phi_{\text{N}2} \approx 1.0$  (eq 1).<sup>49</sup>



Two transient species with decay rate constants of  $1.9 \times 10^8 \text{ s}^{-1}$  ( $\tau = 5.2$  ns, light green) and  $1.5 \times 10^5 \text{ s}^{-1}$  ( $\tau = 6.8 \mu\text{s}$ , light blue) were observed in the sub-nanosecond TA spectroscopic analysis of AZ-6CPP (Figure 4a,b). The slow decay rate constant is consistent with that obtained in the sub-microsecond TA analysis ( $\tau = 6.5 \mu\text{s}$ , Figure 4b, light blue). The absorption spectrum of short-lived species was obtained by subtracting the spectrum at 100 ns from that at 1 ns (Figure 4c, light green). The short-lived species with  $\tau = 5.2$  ns has an absorption maximum at approximately 590 nm. The transient species is assigned to the singlet excited state  $S_1$  because the lifetime of 5.2 ns is consistent with that of the fluorescence lifetime,  $\tau_f = 5.0$  ns, as shown in Figure 3f. After approximately 20 ns, another TA spectrum was obtained, and this contained absorption peaks at 540 and 660 nm (Figure 4a, light blue)

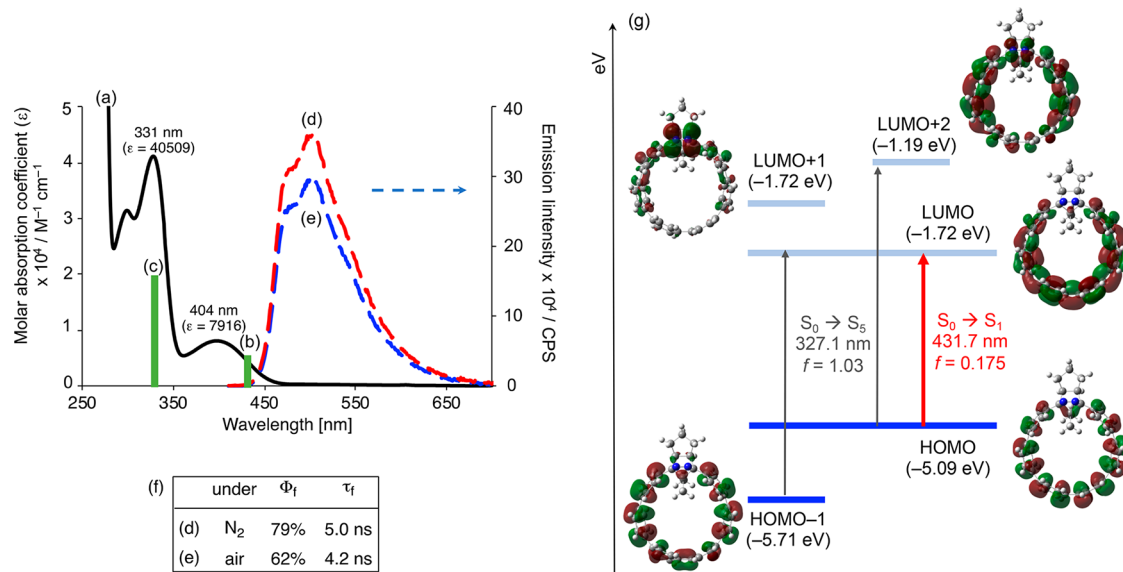


**Figure 3.** Absorption and emission analysis of AZ-6CPP in benzene: (a) UV-vis absorption spectrum; (b) computed  $S_0 \rightarrow S_1$  transition ( $\lambda_{\text{calc}} = 431.7 \text{ nm}, f = 0.175$ ) at the TD-B3LYP/6-31G(d) level of theory; (c) computed  $S_0 \rightarrow S_5$  transition ( $\lambda_{\text{calc}} = 327.1 \text{ nm}, f = 1.03$ ) at the TD-B3LYP/6-31G(d) level of theory; (d) emission spectrum for 400 nm excitation ( $\text{Abs}_{400} = 0.1$ ) under an  $N_2$  atmosphere in benzene solution; (e) emission spectrum for 400 nm excitation under air in benzene solution; (f) emission quantum yield ( $\Phi_f$ ) and lifetime ( $\tau_f$ ) in  $N_2$  and air; (g) energy diagram of Kohn–Sham orbitals and electronic transitions computed at the TD-B3LYP/6-31G(d) level of theory.

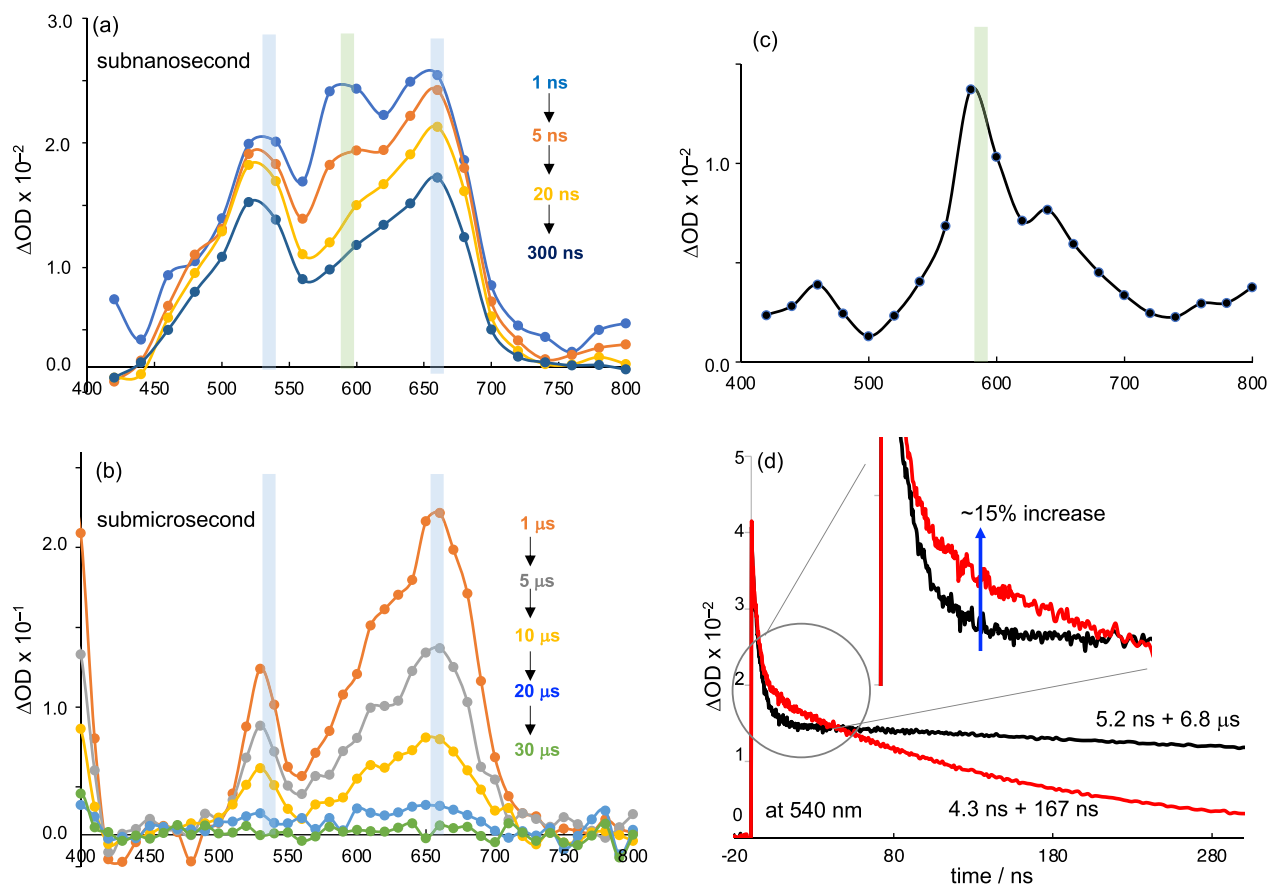


**Figure 4.** Time-resolved transient absorption spectra during the photolysis of AZ-6CPP in benzene: (a) sub-nanosecond time-resolved transient absorption spectra in benzene under an Ar atmosphere (355 nm, 80  $\mu\text{J}/\text{pulse}$ , 25 ps pulse width) at 295 K; (b) sub-microsecond time-resolved transient absorption spectra in benzene under a  $N_2$  atmosphere (355 nm, 6 mJ/pulse, 4 ns pulse width) at 295 K; (c) transient absorption spectrum of short-lived species (singlet excited state) with  $\tau = 5.2 \text{ ns}$  obtained by subtracting the spectrum at 100 ns from that at 1 ns; (d) time profile at 540 nm in the sub-nanosecond time-resolved spectroscopic analysis in Ar (black) and air (red).

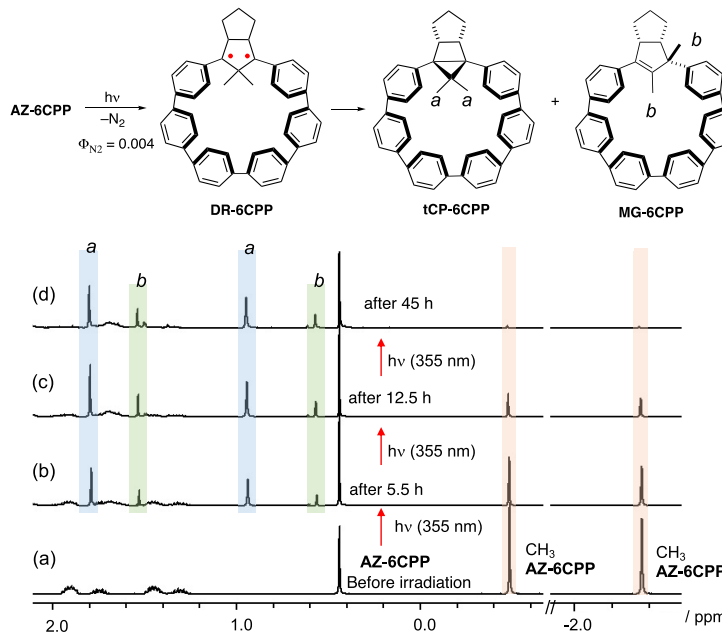
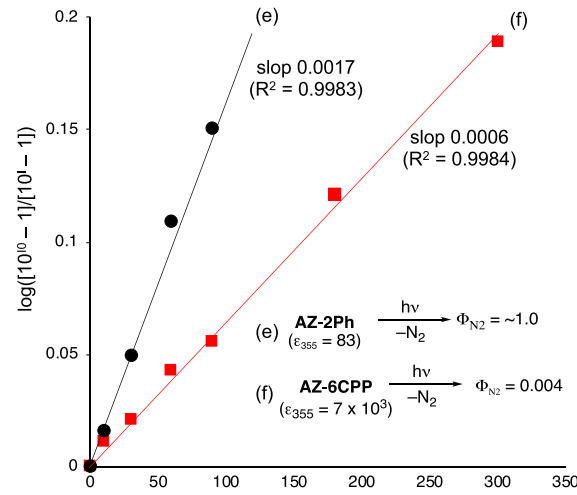


**Figure 5.**  $^1H$  NMR analysis (400 MHz) of the photolysis of AZ-6CPP (20 mM) by 355 nm laser (5.5 mJ/pulse) in degassed  $C_6D_6$  solution: (a) before irradiation; (b) after 2 h irradiation; (c) after 12.5 h irradiation; (d) after 45 h irradiation. Time profiles of the decomposition of azoalkanes (e) AZ-2Ph and (f) AZ-6CPP as monitored by  $^1H$  NMR spectroscopy using a 355 nm laser (5.5 mJ).

that could be assigned to the triplet state ( $T_1$ ). Indeed, the lifetime of the species detected at 540 nm was significantly shortened to about 167 ns in air (Figure 4d, red). A careful analysis of the triplet TA spectrum at 540 nm revealed that the fluorescence quenching observed in the fluorescence measurements in Figure 3e is due to an increase in the intersystem crossing (ISC) from the  $S_1$  to the  $T_1$  state in the presence of  $^3O_2$  because the intensity of the triplet TA in air was approximately 15% higher than that obtained in Ar (Figure 4d).

**Product Analysis of the Photolysis of AZ-6CPP.** As found in the TA analysis, the quantum yield for the denitrogenation of AZ-6CPP is too low to allow detection of the diradical intermediate DR-6CPP directly using a time-resolved spectroscopic analysis. To confirm the denitrogenation of AZ-6CPP, the photoreaction of AZ-6CPP (20 mM) using a 355 nm yttrium aluminum garnet (YAG) laser (approximately 5.5 mJ/pulse) was monitored by  $^1H$  NMR spectroscopy at 295 K in degassed  $C_6D_6$  solution in a sealed NMR tube under vacuum conditions (Figure 5). During the irradiation of AZ-6CPP, two new pairs of  $CH_3$  groups (*a*, 0.95 and 1.82 ppm; *b*, 0.58 and 1.52 ppm; Figure 5) were observed in the photolysate with the concomitant decrease of two  $CH_3$  groups of AZ-6CPP (-2.36 and -0.49 ppm). After 45 h of irradiation (Figure 5d), AZ-6CPP was almost completely consumed under the photolysis conditions. The photoproducts were purified by column chromatography on silica gel. Both of these products were thermally labile and gradually decomposed under air conditions. Using quick column chromatography, the separated samples were sealed under  $N_2$  and analyzed by  $^1H$  NMR, 2D NMR, 2D-nuclear Overhauser effect (NOESY), and mass spectroscopy, demonstrating that the photoreaction products *a* and *b* are the *trans*-configured ring-closed compound tCP-6CPP and a methyl-group-migrated alkene product (MG-6CPP), respectively (Figures S29–S47).



The denitrogenation quantum yield ( $\Phi_{N_2}$ ) of AZ-6CPP was determined by comparing the decomposition rate with that of AZ-2Ph, whose denitrogenation quantum yield is known to be 1.0.<sup>49</sup> The decomposition of azoalkanes was monitored by  $^1H$  NMR spectroscopy (Figure 5e,f). The function  $\log([10^I - 1]/[10^I - 1])$ , where  $I$  is the  $^1H$  NMR signal intensity of the  $CH_3$  groups in AZ-6CPP and AZ-2Ph (Figures S27 and S28), increased linearly with irradiation time using a laser wavelength of 355 nm. The photoreaction quantum yield of AZ-6CPP was calculated from the ratio of the slopes of AZ-6CPP/AZ-2Ph =  $\epsilon_{AZ-6CPP}\Phi_{N_2}/\epsilon_{AZ-2Ph}\Phi_{N_2}$ , where  $\epsilon_{AZ-6CPP}$  ( $7 \times 10^3 M^{-1} cm^{-1}$ ) and  $\epsilon_{AZ-2Ph}$  ( $83 M^{-1} cm^{-1}$ ) are the molar extinction coefficients of AZ-6CPP and AZ-2Ph at 355 nm, respectively. From the analysis, the denitrogenation quantum yield of AZ-6CPP was determined to be 0.004 (0.4%). The low quantum yield is a result of the 355 nm light being mainly absorbed by the curved  $\pi$ -conjugated moiety, as suggested by the TA analysis (Figure 4).

**EPR Measurements.** Although the quantum yield of the photochemical denitrogenation of AZ-6CPP is very low, it might be possible to observe DR-6CPP directly during the photolysis of AZ-6CPP using an electron paramagnetic resonance (EPR) spectroscopic analysis because of its high sensitivity to paramagnetic species. Thus, low-temperature photolysis of AZ-6CPP (11 mM) in degassed 2-methyltetrahydrofuran (2MTHF) was conducted using a Hg lamp ( $\lambda_{emi} > 250$  nm) at 4 K (Figure 6). After 4 h, a typical signal stemming from persistent triplet species was observed at 1650 G, and this was assigned to the  $\Delta M_S = \pm 2$  forbidden transition. In addition to the half-field signal at 1650 G, the allowed transitions of  $\Delta M_S = \pm 1$  (2977 ( $z_1$ ), 3142 ( $xy_1$ ), 3560 ( $xy_2$ ), and 3731 G ( $z_2$ )) were observed at a resonance frequency of 9.40 GHz. From the  $z$  signals, the zero-field splitting (zfs) parameters were determined to be  $|D|/h\gamma = 0.035 cm^{-1}$  and  $|E|/h\gamma \leq 0.001 cm^{-1}$  (Figure 6a).<sup>13</sup> The triplet EPR spectrum was consistent with the simulated spectrum by inputting zfs

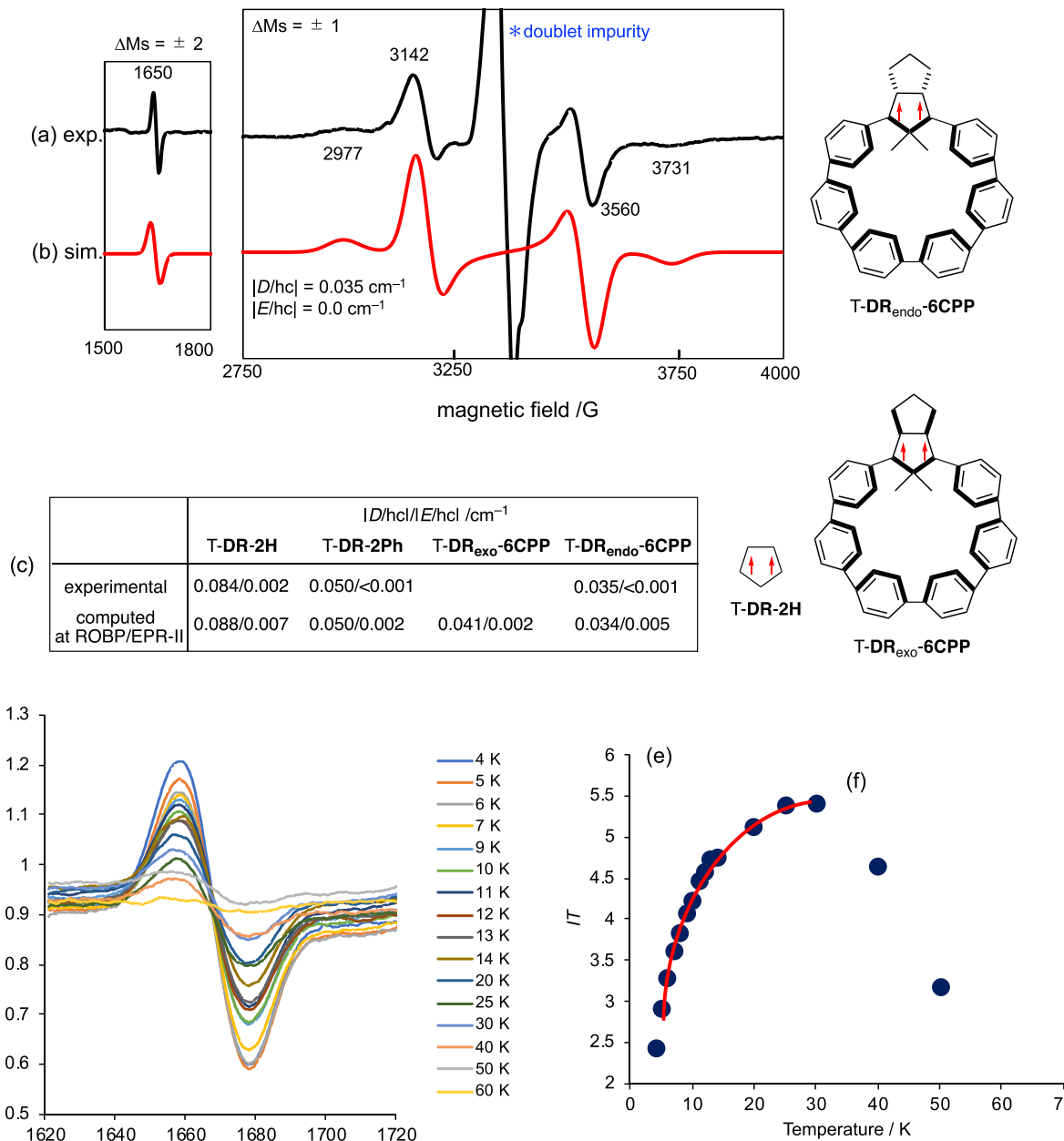


**Figure 6.** (a) EPR spectrum of the photolysis of AZ-6CPP (11 mM) using an Hg lamp (>250 nm) in 2MTHF matrix in a sealed quartz tube at 4 K under vacuum conditions (resonance frequency 9.40 GHz). (b) EPR spectrum simulated using the zfs parameters  $|D/hc| = 0.035 \text{ cm}^{-1}$  and  $|E/hc| = 0.00 \text{ cm}^{-1}$ . (c) Experimental and computed zfs parameters ( $D$  and  $E$ ) for diradicals T-DR-2H, T-DR-2Ph, and T-DR<sub>endo</sub>-6CPP. (d) Temperature dependence of the intensity of the EPR signal at 1650 G. (e)  $IT-T$  plot. (f) Least-squares fit for the Bleaney–Bowers analysis.

parameters of  $|D/hc| = 0.035 \text{ cm}^{-1}$  and  $|E/hc| = 0 \text{ cm}^{-1}$  (Figure 6b), and the average distance between the two dipoles was determined to be 4.20 Å using the point dipole approximation,<sup>50</sup> which is longer than 3.76 Å in DR-2Ph ( $|D/hc| = 0.050 \text{ cm}^{-1}$  and  $|E/hc| \leq 0.001 \text{ cm}^{-1}$ )<sup>51,52</sup> generated from AZ-2Ph (eq 1), indicating that the diradical is more delocalized over the benzene rings.<sup>51</sup>

To obtain more information about the triplet diradical generated in the photolysis of AZ-6CPP, the spin densities of diradicals T-DR-2Ph and T-DR<sub>endo</sub>-6CPP were computed at the UB3LYP/6-31G(d) level of theory. The spin density at the benzylic carbon of T-DR-2Ph was computed to be 0.753. The corresponding value for T-DR<sub>exo</sub>-6CPP was calculated to be

0.706. A smaller value of 0.665 was found for the endo isomer, T-DR<sub>endo</sub>-6CPP. To confirm the structural assignment of the triplet diradical having a smaller  $D$  value ( $|D/hc| = 0.035 \text{ cm}^{-1}$ ) in comparison to that of DR-2Ph ( $|D/hc| = 0.050 \text{ cm}^{-1}$ ), the zfs parameters  $D$  and  $E$  were computed at the (RO)BP/EPR-II//UB3LYP/6-31G(d)<sup>53,54</sup> level of theory using ORCA 4.2.1<sup>55,56</sup> (Figure 6c). The zfs parameters of the parent triplet diradical T-DR-2H ( $|D/hc| = 0.084 \text{ cm}^{-1}$  and  $|E/hc| = 0.002 \text{ cm}^{-1}$ )<sup>57,58</sup> were also calculated at the same level of theory to confirm the reliability of the computation. As shown in Figure 6c, the experimentally obtained  $|D/hc|$  values in wavenumbers, 0.084 and 0.050  $\text{cm}^{-1}$  for T-DR-2H and T-DR-2Ph, respectively, were well reproduced by the computations: i.e.,

0.088 and  $0.050\text{ cm}^{-1}$ , respectively. The  $D$  values for  $\text{T-DR}_{\text{exo}}\text{-6CPP}$  and  $\text{T-DR}_{\text{endo}}\text{-6CPP}$  were computed to be 0.041 and  $0.034\text{ cm}^{-1}$ , respectively. Thus, the triplet signals observed in the photolysis of **AZ-6CPP** (Figure 6a) were assigned to  $\text{T-DR}_{\text{endo}}\text{-6CPP}$ . Although  $\text{T-DR}_{\text{endo}}\text{-6CPP}$  was calculated to be less stable than  $\text{T-DR}_{\text{exo}}\text{-6CPP}$  by  $7.9\text{ kcal mol}^{-1}$ , the assignment is reasonable because **AZ-6CPP** (Scheme 1) has the same configuration as the endo isomer  $\text{DR}_{\text{endo}}\text{-6CPP}$ , featuring a *trans* configuration of the dimethylmethano moiety with the cyclopentane ring.

The temperature dependence of the intensity of the triplet signal at  $1650\text{ G}$  was examined to determine the ground-state spin multiplicity. The intensity measurements were conducted at a microwave power of  $20\text{ mW}$ , for which signal saturation was not observed, even at  $4\text{ K}$  (Figure S82). After the generation of **DR-6CPP** at  $4\text{ K}$ , the temperature was increased by 1 to  $15\text{ K}$  and then by  $5\text{ K}$  until  $30\text{ K}$  (Figure 6d). Surprisingly, the triplet signal suddenly weakened at  $40\text{ K}$  (Figure 6d) and the signal intensity did not return to the original intensity at  $4\text{ K}$ . After regeneration of **DR-6CPP** at  $6\text{ K}$ , the sample was heated to  $30\text{ K}$  and then recooled to  $6\text{ K}$  to confirm the thermal stability of **DR-6CPP** at  $30\text{ K}$ . The intensity of  $0.545$  at  $6\text{ K}$  before the sample was warmed was nearly the same as  $0.547$  at  $6\text{ K}$  after the sample was recooled to  $6\text{ K}$  (Figure S83), suggesting that **DR-6CPP** is persistent below  $30\text{ K}$ . The high reactivity, even at  $40\text{ K}$ , is significantly different from the persistent character of **T-DR-2Ph** at  $77\text{ K}$ .<sup>59</sup> In the  $IT-T$  plot below  $30\text{ K}$  (Figure 6d), the  $IT$  value gradually decreased with decreasing temperature, indicating that the triplet state is thermally populated as an excited state. From the least-squares fit for the Bleaney–Bowers analysis ( $R^2 = 0.9825$ , number of points 14, Figure 6e,f),<sup>60</sup> the singlet ( $E_S$ )–triplet ( $E_T$ ) energy gap ( $\Delta E_{\text{ST}} = 2J/k_B = E_S - E_T; J/k_B$  is the exchange interaction) was determined to be  $-15.8 \pm 0.5\text{ cal mol}^{-1}$  ( $=-7.9\text{ K}, J/k_B = 3.95\text{ K}$ ), demonstrating the singlet ground state of  $\text{DR}_{\text{endo}}\text{-6CPP}$  (Figure 6e). Thus, the ground-state spin multiplicity was switched by the curved macrocyclic structure. The maximum in the  $I-T$  plot (Figure S84) was not clearly observed in the temperature range of  $4$ – $30\text{ K}$  because the exchange interaction value was  $J/k_B = 3.95\text{ K}$ .

## DISCUSSION

As found in the EPR experiments, the ground-state spin multiplicity switched from triplet in **DR-2Ph** to singlet in **DR<sub>endo</sub>-6CPP**, which has a curved  $\pi$ -conjugated structure, although the singlet–triplet energy spacing is small. To gain more insight into the macrocyclic effect, the singlet–triplet energy spacings of **DR-2Ph**, **DR<sub>endo</sub>-6CPP**, and **DR<sub>endo</sub>-2Ph'** were computed using DFT (CAM-B3LYP/6-31G(d))<sup>61</sup> and complete active space self-consistent field (CASSCF)<sup>62</sup> calculations in Gaussian 16.<sup>63</sup> The structure of **DR<sub>endo</sub>-2Ph'** was obtained by replacing the middle four benzene rings with two hydrogen atoms in **DR<sub>endo</sub>-6CPP** without optimizing the curved structure of the two benzene rings at the radical sites (Figure 7c). The open-shell singlet state was computed using the broken-symmetry (BS)<sup>64</sup> approach for the DFT calculations. The energy corrections were conducted using the complete active space second-order perturbation theory (CASPT2)<sup>65</sup> for the CASSCF calculations. Thus, the effect of the curvature on the open-shell singlet–triplet energy spacing was appropriately computed.

First, the molecular structures **DR-2Ph** and **DR<sub>endo</sub>-6CPP** were optimized at the BS-UCAM-B3LYP/6-31G(d) level of

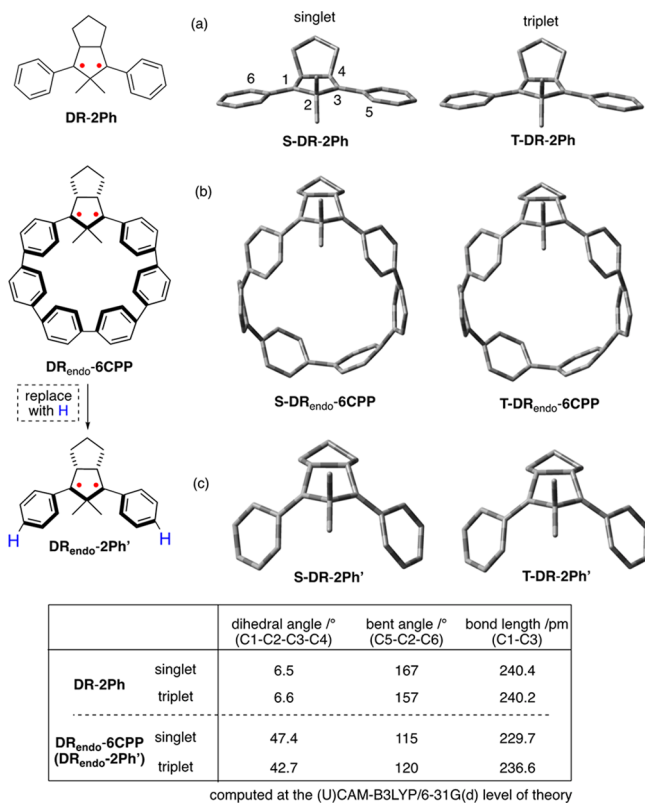


**Figure 7.** Structures of (a) **DR-2Ph**, (b) **DR<sub>endo</sub>-6CPP**, and (c) **DR<sub>endo</sub>-2Ph'** optimized at the UCAM-B3LYP/6-31G(d) level of theory. Hydrogen atoms are omitted for clarity.

theory. Nearly planar structures were found in the cyclopentane-1,3-diyl moiety for **DR-2Ph** (Figure 7a), and the C1–C2–C3–C4 dihedral angles were computed to be approximately  $6.5^\circ$  for both triplet and singlet states. The two planar benzene rings have a coplanar orientation with the cyclopentane-1,3-diyl moiety, as shown by the C5–C2–C6 angles, which were calculated to be  $167$  and  $157^\circ$  for the singlet and triplet states, respectively. The distances between C1 and C3 were found to be  $240.4$  and  $240.2\text{ pm}$  in the singlet and triplet states, respectively. Thus, nearly the same molecular structures were found in the singlet and triplet states of **DR-2Ph**.

In contrast to the planar and flat structures of **DR-2Ph**, puckered and bent structures were found in **DR<sub>endo</sub>-6CPP** at the same level of theory (Figure 7b). Puckered structures having C1–C2–C3–C4 dihedral angles of  $47.4$  and  $42.7^\circ$  were obtained for the singlet and triplet **DR<sub>endo</sub>-6CPP**, respectively (Figure 7b). The C5–C2–C6 angles (bending of the benzene rings) in the singlet and triplet states of **DR<sub>endo</sub>-6CPP** were computed to be  $115$  and  $120^\circ$ , respectively, which are smaller than that of **DR-2Ph** ( $\sim 160^\circ$ ). In particular, the atomic distance of  $229.7\text{ pm}$  in **S-DR<sub>endo</sub>-6CPP** was significantly shorter than that in the triplet state **T-DR<sub>endo</sub>-6CPP** ( $236.6\text{ pm}$ ) and in the singlet and triplet states in **DR-2Ph** ( $240.4$  and  $240.2\text{ pm}$ ).

To understand the electronic structures of **DR-2Ph** and **DR<sub>endo</sub>-6CPP**, the HOMO and LUMO occupation numbers in their singlet states were compared (Figure 8). The occupation numbers of **S-DR-2Ph** and **S-DR<sub>endo</sub>-6CPP** were determined at the CASSCF(2,2)/6-31G(d) level of theory. As clearly shown in the HOMO and LUMO images (Figure 8a), a parallel alignment of the p orbitals was found in **S-DR-2Ph**. The

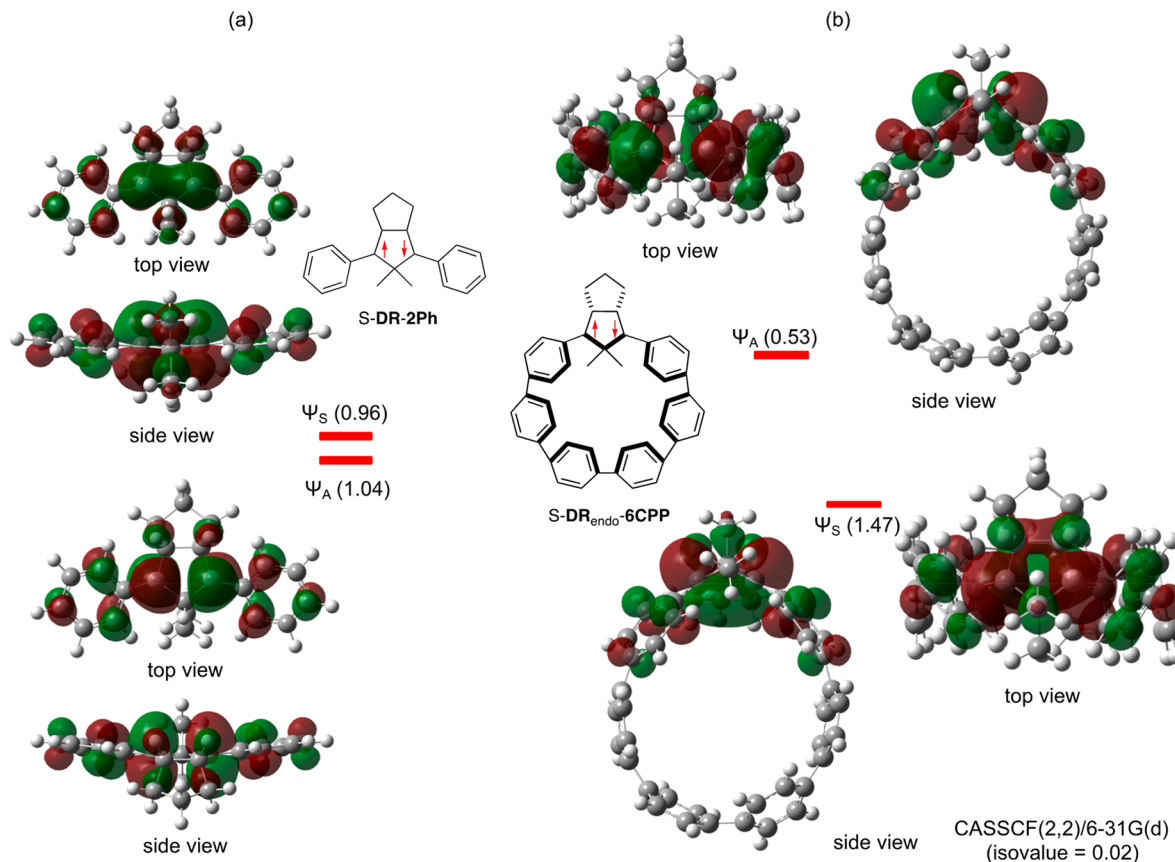


**Figure 8.** HOMO and LUMO orbitals and their occupation numbers in (a) S-DR-2Ph and (b) S-DR<sub>endo</sub>-6CPP calculated at the CASSCF(2,2)/6-31G(d) level of theory.

**Table 1. Singlet–Triplet Energy Gap ( $\Delta E_{ST} = E_S - E_T$ ) in DR-2Ph, DR<sub>endo</sub>-6CPP, and DR-2Ph'**

entry	diradical	singlet–triplet energy gap/kcal mol <sup>-1</sup> ( $\Delta E_{ST} = E_S - E_T$ )		
		UCAM-B3LYP/6-31G(d)	CASSCF(14,14)/cc-pVDZ	CASPT2(14,14)/cc-pVDZ
1	DR-2Ph	+0.20	+0.37	+0.20
2	DR <sub>endo</sub> -6CPP	-1.77	nd	nd
3	DR-2Ph'	-1.20	-3.84	-6.35

occupation numbers of electrons in the HOMO ( $\psi_A$ ) and LUMO ( $\psi_S$ ) orbitals in S-DR-2Ph were computed to be 1.04 and 0.96, respectively, indicating a negligible bonding interaction between the two radicals: that is, nearly pure singlet diradical character in S-DR-2Ph. Thus, the triplet ground state is reasonable for DR-2Ph. In contrast, a bent conformation was found in S-DR<sub>endo</sub>-6CPP, which suggests a bent-type (banana-like) bonding interaction between the two radical sites (Figure 8b). Indeed, S-DR<sub>endo</sub>-6CPP possesses a bonding combination of HOMO ( $\psi_S$ ) and antibonding LUMO ( $\psi_A$ ), whose orbital order is, interestingly, opposite in S-DR-2Ph (Figure 8a). The switch in the HOMO–LUMO conversion in DR-2Ph is a result of through-bond interactions.<sup>12,25,66–70</sup> The occupation numbers in the bonding ( $\psi_S$ ) and antibonding ( $\psi_A$ ) orbitals were found to be 1.47 and 0.53, respectively, and the bond order between the radical sites was calculated to be 0.47 from the occupation numbers in the bonding and antibonding orbitals.

The singlet–triplet energy spacing in DR-2Ph and DR<sub>endo</sub>-6CPP was computed at the UCAM-B3LYP/6-31G(d) level of theory (Table 1). In contrast to the triplet ground state of diradicals DR-2Ph,  $\Delta E_{ST} = E_S - E_T = +0.20$  kcal mol<sup>-1</sup>, the

singlet was calculated to be the ground state, having an energy preference of 1.77 kcal mol<sup>-1</sup>, in DR<sub>endo</sub>-6CPP (entries 1 and 2). To confirm the energy gap obtained in the DFT calculations, the DR-2Ph' diradical having curved benzene rings was used for the computation of the energy gap at the CASPT2(14,14)/cc-pVDZ level of theory using OpenMolcas<sup>71</sup> because the  $\pi$ -electrons in DR-6CPP are too large to allow computation of the energy gap using the CASPT2 method. A singlet ground state with  $\Delta E_{ST} = E_S - E_T = -3.84$  and -6.35 kcal mol<sup>-1</sup> was found for DR<sub>endo</sub>-2Ph' at the CASSCF(14,14)/cc-pVDZ and CASPT2(14,14)/cc-pVDZ levels of theory, respectively (entry 3). At the same level of theory, the triplet ground state was confirmed, having  $\Delta E_{ST} = +0.20$  kcal mol<sup>-1</sup>, for DR-2Ph (entry 1). Thus, the singlet preference of DR<sub>endo</sub>-6CPP (Figure 6e) is rationalized to result from the puckered structure of the diradical. The bent-bonding interaction between the two radical sites is the key reason for the singlet ground state in S-DR<sub>endo</sub>-6CPP (Figure 8b).

To obtain more insights into the macrocyclic effect on the reactivity of the diradicals, the ring-closing reaction to yield CP-6CPP was computed, thus allowing comparison with the corresponding reaction for DR-2Ph (Figure 9). First, the ring-

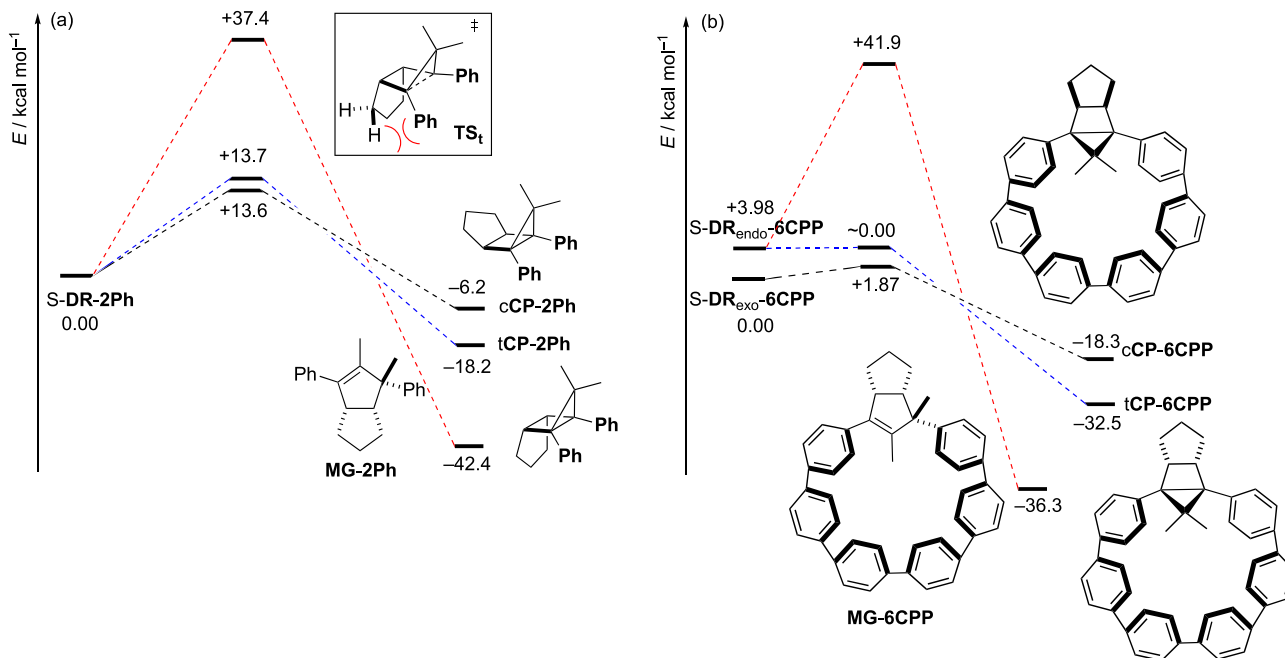


**Figure 9.** Computations on the thermal reactivity of singlet diradicals S-DR-2Ph and S-DR-6CPP at the (U)CAM-B3LYP/6-31G(d) level of theory.

closing reaction of S-DR-2Ph to CP-2Ph was computed at the BS-(U)CAM-B3LYP/6-31G(d) level of theory. The kinetically favored ring-closing reaction was found to give a *cis*-configured compound, cCP-2Ph, with an energy barrier of 13.6 kcal mol<sup>-1</sup> (Figure 9a). A slightly high energy barrier, 13.7 kcal mol<sup>-1</sup>, was calculated for the reaction to the *trans*-configured compound, tCP-2Ph. The repulsive interaction between Ph and CH<sub>2</sub> groups in the transition state TSt increases the energy of TSt for the formation of tCP-2Ph, whose observation is similar to that of the previously reported kinetically favored formation of a *cis* isomer.<sup>72</sup> The persistent character of DR-2Ph at low temperature (<100 K) is reasonable on the basis of the relatively large energy barriers for the radical–radical coupling reaction obtained by computation.

A small energy barrier, 1.87 kcal mol<sup>-1</sup>, was calculated for the ring-closing reactions in the exo isomer of S-DR-6CPP, S-DR<sub>exo</sub>-6CPP (black line, Figure 9b). In the reaction of endo isomer S-DR<sub>endo</sub>-6CPP, a clear energy barrier was not found during the scan calculation in the C1–C3 bond-formation process to give the ring-closed compound tCP-6CPP (Figure S88); thus, the energy barrier from S-DR<sub>endo</sub>-6CPP to tCP-6CPP is should be very small (blue line, Figure 9b). The observed high reactivity of DR<sub>endo</sub>-6CPP, even at 40 K, under low-temperature matrix conditions is reasonable because of the very small energy barrier. In the photolysis of AZ-6CPP, another product, MG-6CPP, was formed (Figure 6). A relatively large energy barrier of 41.9 kcal mol<sup>-1</sup> was computed for the methyl migration reaction in S-DR<sub>endo</sub>-6CPP (red line, Figure 9b), which is much higher in energy than that of the ring-closing reaction. The large energy barrier computed for the migration reaction suggests that the formation of MG-6CPP stems from an electronically excited state. Photolysis of the matrix-isolated DR-2Ph has been reported to produce the corresponding methyl migration product, MG-2Ph.<sup>59</sup> The photolysis of tCP-2Ph using 266 nm irradiation, indeed produced MG-2Ph (Figures S85–S87). Thus, compound MG-

6CPP is proposed to be formed in the secondary photo-reaction of CP-6CPP.

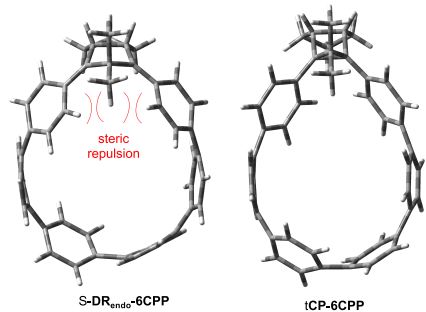
We wondered “why are the energy barriers from S-DR<sub>endo</sub>-6CPP to tCP-6CPP and from S-DR<sub>exo</sub>-6CPP to cCP-6CPP so small?” As shown in Figure 8b, the puckered structure of S-DR<sub>endo</sub>-6CPP, which already possesses a bent-bonding character, is one of the reasons for the small energy barrier. Similar molecular structures were found in S-DR<sub>exo</sub>-6CPP (Figure S135). To gain more insight into the high reactivity of DR-6CPP, the molecular strain energies were computed for AZ-6CPP, S-DR<sub>endo</sub>-6CPP, T-DR<sub>endo</sub>-6CPP, S-DR<sub>exo</sub>-6CPP, T-DR<sub>exo</sub>-6CPP, tCP-6CPP, and cCP-6CPP using eq 2 in Table 2. The strain energies of AZ-6CPP and DR-6CPP were determined to be 79–85 kcal mol<sup>-1</sup> (entries 1–5), similar to that of [7]CPP (84 kcal mol<sup>-1</sup>)<sup>73</sup> calculated at the B3LYP/6-31G(d) level of theory. The strain energy of DR<sub>endo</sub>-6CPP was higher by ~5 kcal mol<sup>-1</sup> than that of the exo isomer (entries 2–5). Surprisingly, the strain energies of the ring-closed CP-6CPP were found to be approximately 10 and 15 kcal mol<sup>-1</sup> lower than those of the diradical intermediates S-DR<sub>exo</sub>-6CPP and S-DR<sub>endo</sub>-6CPP, respectively (entries 6 and 7), although the ring size of CP-6CPP is, in principle, smaller than that of DR-6CPP by one carbon. The computational results demonstrate that the ring-closing reaction releases molecular strain, suggesting that the small energy barriers in the ring-closing process in DR-6CPP were accelerated by the release of molecular strain, as well as the bonding interaction in S-DR-6CPP. A question quickly arises: “Why is the molecular strain in CP-6CPP smaller than that in DR-6CPP in spite of the smaller ring size in CP-6CPP in comparison to that in DR-6CPP?” A careful analysis of the optimized structures revealed that there is greater steric repulsion between the methyl group and the adjacent benzene ring in S-DR-6CPP in comparison to that in cCP-6CPP because the phenyl ring can twist in CP-6CPP (see the optimized structures in Table 2).

As shown by pioneering studies on the effects of size on the electronic character of CPPs,<sup>33,35</sup> the size-dependent change in

**Table 2.** Molecular Strain Energies of AZ-6CPP, S-DR<sub>endo</sub>-6CPP, T-DR<sub>endo</sub>-6CPP, tCP-6CPP, and cCP-6CPP at the (U)CAM-B3LYP/6-31G(d) Level of Theory

Reaction scheme (2) illustrates the synthesis of larger macrocyclic molecules from smaller building blocks. On the left, three molecules are shown: AZ-6CPP, DR-6CPP, and CP-6CPP. An arrow points to the right, where these are converted into AZ-2Ph, DR-2Ph, and CP-2Ph. These intermediate molecules are then used to form larger macrocyclic structures. Specifically, six AZ-2Ph units are joined together, and seven DR-2Ph units are joined together. The resulting macrocycles are labeled with their respective names: S-DR<sub>endo</sub>-6CPP, T-DR<sub>endo</sub>-6CPP, S-DR<sub>exo</sub>-6CPP, T-DR<sub>exo</sub>-6CPP, tCP-6CPP, and cCP-6CPP. The strain energy values for each molecule are listed in Table 2.

entry	molecule	strain energy/kcal mol <sup>-1</sup>
1	AZ-6CPP	78.8
2	S-DR <sub>endo</sub> -6CPP	82.6
3	T-DR <sub>endo</sub> -6CPP	84.6
4	S-DR <sub>exo</sub> -6CPP	78.7
5	T-DR <sub>exo</sub> -6CPP	78.7
6	tCP-6CPP	68.3
7	cCP-6CPP	66.5

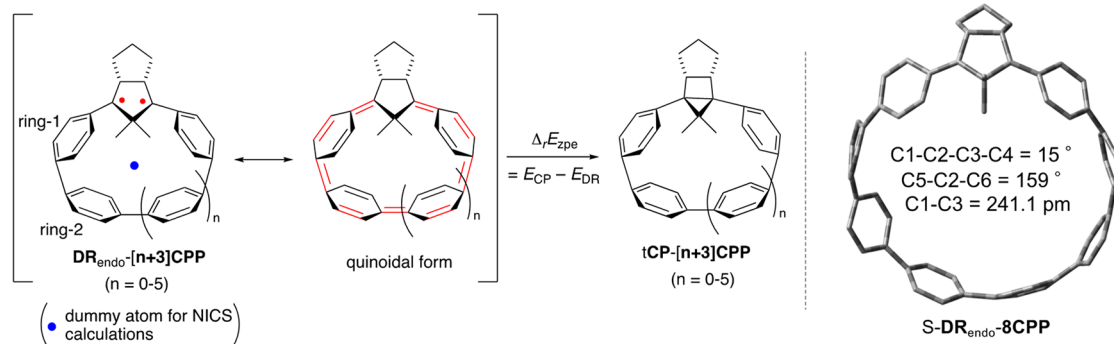


molecular structure and ground-state spin multiplicity is particularly interesting in diradicals embedded in cycloparaphenylenes: DR<sub>endo</sub>-(n+3)CPPs ( $n = 0–5$ ). Thus, the reaction energy ( $\Delta_r E$  in kcal mol<sup>-1</sup>) was computed for the formation of tCP-(n+3)CPP from S-DR<sub>endo</sub>-(n+3)CPPs (Table 3). Interestingly, ring-closed tCP-3CPP was not found to be an equilibrium structure at the restricted B3LYP/6-31G(d) level of theory, and optimization yielded the ring-opened diradical S-DR<sub>endo</sub>-3CPP featuring the quinoidal form (entry 1). Thus, the intramolecular cyclization of S-DR<sub>endo</sub>-3CPP to tCP-3CPP is energetically disfavored, although the strain energy (SE) of S-DR<sub>endo</sub>-3CPP was computed to be high: SE<sub>DR</sub> = 91.3 kcal mol<sup>-1</sup>. The exothermicity ( $\Delta_r E$ ) of the intramolecular cyclization is prone to increase with increasing size ( $n$ ) of the paraphenylene moiety (entries 2–6). The strain energies (SE<sub>CP</sub> and SE<sub>DR</sub>) in tCP-(n+3)CPP and S-DR<sub>endo</sub>-(n+3)CPP were found to decrease with increasing macrocyclic ring size (entries 2–6). The strain energy (SE<sub>DR</sub>) in S-DR<sub>endo</sub>-3CPP was smaller than that in S-DR<sub>endo</sub>-4CPP (entries 1 and 2). The quinoidal form of S-DR<sub>endo</sub>-3CPP would be the reason for this.

The effect of the ring size on the singlet–triplet energy gap ( $\Delta E_{ST} = E_S - E_T$ ) computed at the (U)CAM-B3LYP/6-31G(d) level of theory was also analyzed in DR<sub>endo</sub>-(n+3)CPP, and the results are summarized in Table 3. Interestingly, the energy gap was found to be significantly dependent on the ring size. In particular, as the size of the rings increases, there is a tendency for the triplet state to become more stable. For example, a significant preference (by 21.3 kcal mol<sup>-1</sup>) for the

singlet state was found for DR-3CPP ( $n = 0$ , entry 1), whereas the triplet ground state was computed for DR<sub>endo</sub>-7CPP ( $n = 4$ , entry 5) and DR<sub>endo</sub>-8CPP ( $n = 5$ , entry 6). It should be noted that the singlet–triplet energy gap drastically increased to 4.5 and 21.3 kcal mol<sup>-1</sup> (i.e., singlet preference) for DR<sub>endo</sub>-4CPP and DR<sub>endo</sub>-3CPP, respectively (entries 1 and 2). The singlet states of DR<sub>endo</sub>-3CPP and DR<sub>endo</sub>-4CPP are not perfect open-shell molecules; rather, they are nearly closed-shell molecules (quinoidal structures) because the occupation numbers in HOMOs of S-DR<sub>endo</sub>-3CPP and S-DR<sub>endo</sub>-4CPP were computed to be 1.91 and 1.64 at the CASSCF(2,2)//BS-UCAM-B3LYP/6-31G(d) level of theory (entries 1 and 2), demonstrating that the quinoidal structures S-DR<sub>endo</sub>-3CPP and S-DR<sub>endo</sub>-4CPP are important. As the size of the rings increases, there is a trend for the singlet state to increase in diradical character, as judged by the occupation numbers of the HOMOs and LUMOs. Finally, a triplet ground state was found for DR<sub>endo</sub>-7CPP and DR<sub>endo</sub>-8CPP due to the small difference in the occupation numbers in the HOMO (1.16 and 1.12) and LUMO (0.84 and 0.88) (Figure 8), having  $\Delta E_{ST} = +0.13$  and  $+0.19$  kcal mol<sup>-1</sup> (entries 5 and 6). Similarly to DR-2Ph (Figure 7), a nearly planar structure having C1–C2–C3–C4 dihedral angles of 22 and 15° and the normal atom distance of C1–C3 (240.4 and 241.1 pm) were found in S-DR<sub>endo</sub>-7CPP and S-DR<sub>endo</sub>-8CPP, respectively.

The quinoidal structure of S-DR<sub>endo</sub>-CPP was evaluated using the harmonic oscillator model of aromaticity (HOMA),<sup>74</sup> which was determined from the bond distances computed in the curved paraphenylene moieties. As shown in entries 1 and 2 of Table 3, the HOMA values of “ring 1” and “ring 2” in the singlet state of DR<sub>endo</sub>-3CPP were found to be significantly smaller than 1.0. As the ring size increased (entries 1–6), the HOMA values approached 1.0. In contrast to the small HOMA values in the singlet states, the corresponding values for the triplet states were found to be much larger than those in the singlet states, even for DR<sub>endo</sub>-3CPP (entry 1). Thus, the singlet state of DR<sub>endo</sub>-3CPP possesses a significant bond-alternating quinoidal form. We realized that the quinoidal structure of the singlet state of S-DR<sub>endo</sub>-(n+3)CPPs would show in-plane aromaticity<sup>75–79</sup> when the homoconjugation<sup>80,81</sup> of two radical sites exists in the macrocyclic structures. The nucleus-independent chemical shift values, NICS(0)<sub>zz</sub> and NICS(0)<sub>iso</sub><sup>82–84</sup> at the center of the ring for the singlet and triplet states were computed to examine the in-plane aromaticity (Table 3). Interestingly, the NICS values were prone to become negative with a decrease in the ring size of the singlet state, indicating that the in-plane aromaticity emerges in the small-sized S-DR<sub>endo</sub>-(n+3)CPPs. The NICS value of S-DR<sub>endo</sub>-4CPP, NICS(0)<sub>zz</sub> (NICS(0)<sub>iso</sub>), was highly negative, -19.2 (-11.1), although the NICS value of the triplet state was found to be +10.4 (-1.0) (entry 2, Figure 10a). The in-plane aromaticity of S-DR<sub>endo</sub>-4CPP was clearly visualized using anisotropy of the induced current density (ACID)<sup>85</sup> plots (Figure 10b,c) and 2D-NICS plots (Figures 10d,e). The smaller negative NICS value of S-DR<sub>endo</sub>-3CPP in comparison to that of S-DR<sub>endo</sub>-4CPP is rationalized by the large bond alternation of the quinoidal structures, which is reflected by the low degree of  $\pi$ -conjugation. As found in the CASSCF calculations, the diradical character increases with an increase in the ring size. Thus, the in-plane aromaticity becomes low for the larger-sized S-DR<sub>endo</sub>-(n+3)CPPs.

**Table 3.** Effect of the Ring Size on the Singlet–Triplet Energy Gap ( $\Delta E_{ST} = E_S - E_T$ ) in DR<sub>endo</sub>-[n+3]CPP (n = 0–5)

entry	DR <sub>endo</sub> -CPP	$\Delta_E = E_{CP} - E_{DR}/\text{kcal mol}^{-1}, \text{SE}_{DR}/\text{SE}_{CP}$	$\Delta E_{ST} = E_S - E_T/\text{kcal mol}^{-1}$	occupation no. in HOMO/LUMO <sup>a</sup>	HOMA (benzene distortion (bent) angle ( $\alpha$ , deg))					
					ring 1		ring 2		NICS(0) <sub>zz</sub> (NICS(0) <sub>iso</sub> ) <sup>b</sup>	
					singlet	triplet	singlet	triplet	singlet	triplet
1	DR <sub>endo</sub> -3CPP	–, 101.0/–	–21.29	1.91/0.09	0.465 (31.8)	0.751 (26.9)	0.541 (30.0)	0.99 (19.3)	–3.6 (–5.5)	+11.9 (–0.8)
2	DR <sub>endo</sub> -4CPP	–25.6, 103.0/95.6	–4.50	1.64/0.36	0.876 (18.5)	0.888 (18.7)	0.971 (18.4)	0.990 (17.2)	–19.2 (–11.1)	+10.4 (–1.0)
3	DR <sub>endo</sub> -5CPP	–31.5, 92.3/79.0	–1.90	1.54/0.46	0.942 (13.3)	0.930 (14.2)	0.993 (12.7)	0.994 (12.6)	–2.9 (–5.2)	+5.2 (–2.3)
4	DR <sub>endo</sub> -6CPP	–32.5, 82.6/68.3	–1.77	1.47/0.53	0.951 (11.8)	0.940 (12.3)	0.995 (9.5)	0.995 (9.7)	+0.1 (–3.5)	+3.6 (–2.2)
5	DR <sub>endo</sub> -7CPP	–35.6, 78.2/60.8	+0.13	1.16/0.84	0.968 (12.1)	0.966 (12.3)	0.995 (8.5)	0.995 (8.6)	+2.4 (–2.1)	+2.9 (–2.0)
6	DR <sub>endo</sub> -8CPP	–35.0, 70.9/54.1	+0.19	1.12/0.88	0.963 (10.7)	0.963 (10.7)	0.995 (8.0)	0.995 (8.1)	+2.1 (–1.7)	+2.3 (–1.6)

<sup>a</sup>Occupation numbers in the HOMOs/LUMOs were determined at the CASSCF(2,2)//BS-UCAM-B3LYP/6-31G(d) level of theory. <sup>b</sup>NICS values at the ring centers were computed at the UB3LYP/6-31+G(d) level of theory.

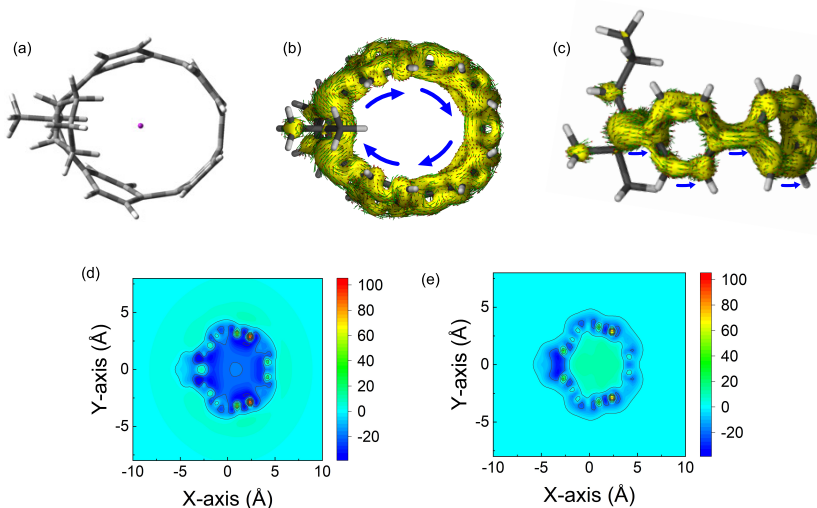


**Figure 10.** (a) Molecular structure of S-DR<sub>endo</sub>-4CPP with a dummy atom at the ring center. (b) Top view and (c) side view of the ACID plot of the ring current in S-DR<sub>endo</sub>-4CPP. 2D-NICS(0)<sub>zz</sub> plots for (d) S-DR<sub>endo</sub>-4CPP and (e) T-DR<sub>endo</sub>-4CPP.

## CONCLUSION

In this study, a novel azoalkane, AZ-6CPP, which is the precursor of DR-6CPP, was synthesized. A relatively high fluorescence quantum yield of 79% was observed for AZ-6CPP because the embedded azo moiety turned on the HOMO–LUMO absorption and emission in the small CPPs via symmetry breaking. The photochemical denitrogenation of AZ-6CPP was carried out to produce the ring-closed

compound tCP-6CPP. The intermediary diradical DR<sub>endo</sub>-6CPP was directly detected using EPR spectroscopic analysis under low-temperature matrix isolation conditions. A singlet ground state was revealed by EPR experiments, although the parent diradical, DR-2Ph, has a triplet ground state. The singlet ground state of DR<sub>endo</sub>-6CPP is rationalized as having a puckered structure in the diradical unit, induced by the curved structure of the paraphenylen moiety. A computational study

on the effects of size on the chemistry of DR<sub>endo</sub>-(n+3)CPP ( $n = 0\text{--}5$ ) demonstrated that (1) the ground-state spin multiplicity is largely dependent on the ring size and the singlet ground state was favored for (3–6)CPP derivatives, (2) in-plane aromaticity emerged for small singlet states such as DR<sub>endo</sub>-4CPP, which involves homoconjugation in the 1,3-diradical moiety, and (3) S-DR<sub>endo</sub>-3CPP is proposed to possess a closed-shell quinoidal structure due to the strongly curved paraphenylenes units. The singlet ground state of small-sized diradicals DR-(n+3)CPP was experimentally proved by the generation of DR-6CPP from AZ-6CPP.

## ■ ASSOCIATED CONTENT

### § Supporting Information

This Supporting Information is available free of charge at The Supporting Information is available free of charge at <https://pubs.acs.org/doi/10.1021/jacs.1c01329>.

Experimental and theoretical details (PDF)

### Accession Codes

CCDC 2060788 contains the supplementary crystallographic data for this paper. These data can be obtained free of charge via [www.ccdc.cam.ac.uk/data\\_request/cif](http://www.ccdc.cam.ac.uk/data_request/cif), or by emailing [data\\_request@ccdc.cam.ac.uk](mailto:data_request@ccdc.cam.ac.uk), or by contacting The Cambridge Crystallographic Data Centre, 12 Union Road, Cambridge CB2 1EZ, UK; fax: +44 1223 336033.

## ■ AUTHOR INFORMATION

### Corresponding Authors

Ivana Antol — Laboratory for Physical Organic Chemistry, Division of Organic Chemistry and Biochemistry, Ruđer Bošković Institute, 10000 Zagreb, Croatia;  
Email: [Ivana.Antol@irb.hr](mailto:Ivana.Antol@irb.hr)

Shigeru Yamago — Institute for Chemical Research, Kyoto University, Uji, Kyoto 611-0011, Japan;  [orcid.org/0000-0002-4112-7249](https://orcid.org/0000-0002-4112-7249); Email: [yamago@scl.kyoto-u.ac.jp](mailto:yamago@scl.kyoto-u.ac.jp)

Manabu Abe — Department of Chemistry, Graduate School of Science, Hiroshima University, Hiroshima 739-8526, Japan;  [orcid.org/0000-0002-2013-4394](https://orcid.org/0000-0002-2013-4394); Email: [mabe@hiroshima-u.ac.jp](mailto:mabe@hiroshima-u.ac.jp)

### Authors

Yuki Miyazawa — Department of Chemistry, Graduate School of Science, Hiroshima University, Hiroshima 739-8526, Japan

Zhe Wang — Department of Chemistry, Graduate School of Science, Hiroshima University, Hiroshima 739-8526, Japan;  [orcid.org/0000-0002-9996-586X](https://orcid.org/0000-0002-9996-586X)

Misaki Matsumoto — Department of Chemistry, Graduate School of Science, Hiroshima University, Hiroshima 739-8526, Japan

Sayaka Hatano — Department of Chemistry, Graduate School of Science, Hiroshima University, Hiroshima 739-8526, Japan

Eiichi Kayahara — Institute for Chemical Research, Kyoto University, Uji, Kyoto 611-0011, Japan;  [orcid.org/0003-1663-5273](https://orcid.org/0003-1663-5273)

Complete contact information is available at:

<https://pubs.acs.org/10.1021/jacs.1c01329>

### Notes

The authors declare no competing financial interest.

## ■ ACKNOWLEDGMENTS

Mass spectrometry measurements were performed at the Natural Science Center for Basic Research and Development (N-BARD) of Hiroshima University. This work was supported by JSPS KAKENHI Grant Numbers 17H03022 (M.A.), 20K21197 (M.A.), and 16H06352 (S.Y.), JST-CREST (Grant Number JPMJCR18R4), and was also supported by the International Collaborative Research Program of Institute for Chemical Research, Kyoto University (grant 2020-43). We thank UNISOKU Co., Ltd., for the use of the picosecond laser system (picoTAS).

## ■ REFERENCES

- (1) Ai, X.; Evans, E. W.; Dong, S.; Gillett, A. J.; Guo, H.; Chen, Y.; Hele, T. J. H.; Friend, R. H.; Li, F. Efficient Radical-Based Light-Emitting Diodes with Doublet Emission. *Nature* **2018**, *563* (7732), 536–540.
- (2) Hattori, Y.; Kusamoto, T.; Nishihara, H. Luminescence, Stability, and Proton Response of an Open-Shell (3,5-Dichloro-4-Pyridyl)Bis-(2,4,6-Trichlorophenyl)Methyl Radical. *Angew. Chem., Int. Ed.* **2014**, *53* (44), 11845–11848.
- (3) Liu, C.; Hamzehpoor, E.; Sakai-Otsuka, Y.; Jadhav, T.; Perepichka, D. F. A Pure-Red Doublet Emission with 90 % Quantum Yield: Stable, Colorless, Iodinated Triphenylmethane Solid. *Angew. Chem., Int. Ed.* **2020**, *59*, 23030–23034.
- (4) Tang, S.; Zhang, L.; Ruan, H.; Zhao, Y.; Wang, X. A Magnetically Robust Triplet Ground State Sulfur-Hydrocarbon Diradical Dication. *J. Am. Chem. Soc.* **2020**, *142*, 7340–7344.
- (5) Gallagher, N. M.; Olankitwanit, A.; Rajca, A. High-Spin Organic Molecules. *J. Org. Chem.* **2015**, *80* (3), 1291–1298.
- (6) Kyushin, S.; Kurosaki, Y.; Otsuka, K.; Imai, H.; Ishida, S.; Kyomen, T.; Hanaya, M.; Matsumoto, H. Silicon-Silicon  $\pi$  Single Bond. *Nat. Commun.* **2020**, *11* (1), 1–7.
- (7) Yıldız, C. B.; Leszczyńska, K. I.; González-Gallardo, S.; Zimmer, M.; Azizoglu, A.; Biskup, T.; Kay, C. W. M.; Huch, V.; Rzepa, H. S.; Scheschkeiwitz, D. Equilibrium Formation of Stable All-Silicon Versions of 1,3-Cyclobutanediyl. *Angew. Chem., Int. Ed.* **2020**, *59* (35), 15087–15092.
- (8) Nukazawa, T.; Iwamoto, T. An Isolable Tetrasilicon Analogue of a Planar Bicyclo[1.1.0]Butane with  $\pi$ -Type Single-Bonding Character. *J. Am. Chem. Soc.* **2020**, *142* (22), 9920–9924.
- (9) Akisaka, R.; Abe, M. Kinetic Stabilization of Localized Singlet Diradicaloids With  $\pi$  Single Bonding Character. In *Kinetic Control in Synthesis and Self-Assembly*; Elsevier: 2019; pp 1–20. DOI: [10.1016/B978-0-12-812126-9.00001-8](https://doi.org/10.1016/B978-0-12-812126-9.00001-8).
- (10) Akisaka, R.; Abe, M. Bulky Substituent Effect on Reactivity of Localized Singlet Cyclopentane-1,3-diyls with  $\pi$ -Single Bonding (C- $\pi$ -C) Character. *Chem. - Asian J.* **2019**, *14* (23), 4223–4228.
- (11) Abe, M.; Akisaka, R. Is  $\pi$ -Single Bonding (C $\pi$ C) Possible? A Challenge in Organic Chemistry. *Chem. Lett.* **2017**, *46* (11), 1586–1592.
- (12) Abe, M.; Ye, J.; Mishima, M. The Chemistry of Localized Singlet 1,3-Diradicals (Biradicals): From Putative Intermediates to Persistent Species and Unusual Molecules with a  $\pi$ -Single Bonded Character. *Chem. Soc. Rev.* **2012**, *41* (10), 3808–3820.
- (13) Abe, M. Diradicals. *Chem. Rev.* **2013**, *113* (9), 7011.
- (14) Ullrich, T.; Pinter, P.; Messelberger, J.; Haines, P.; Kaur, R.; Hansmann, M. M.; Munz, D.; Guldi, D. M. Singlet Fission in Carbene-Derived Diradicaloids. *Angew. Chem., Int. Ed.* **2020**, *59* (20), 7906–7914.
- (15) Kubo, T. Recent Progress in Quinoidal Singlet Biradical Molecules. *Chem. Lett.* **2015**, *44* (2), 111–122.
- (16) Tobe, Y. Non-Alternant Non-Benzoid Aromatic Compounds: Past, Present, and Future. *Chem. Rec.* **2015**, *15* (1), 86–96.
- (17) Dressler, J. J.; Haley, M. M. Learning How to Fine-tune Diradical Properties by Structure Refinement. *J. Phys. Org. Chem.* **2020**, DOI: [10.1002/poc.4114](https://doi.org/10.1002/poc.4114).

- (18) Mori, S.; Akita, M.; Suzuki, S.; Asano, M. S.; Murata, M.; Akiyama, T.; Matsumoto, T.; Kitamura, C.; Kato, S. Open-Shell Singlet Diradicaloid Difluoreno[4,3-b:3',4'-d]Furan and Its Radical Cation and Dianion. *Chem. Commun.* **2020**, *56* (44), 5881–5884.
- (19) Sahara, K.; Abe, M.; Zipse, H.; Kubo, T. Duality of Reactivity of a Biradicaloid Compound with an O-Quinodimethane Scaffold. *J. Am. Chem. Soc.* **2020**, *142* (11), 5408–5418.
- (20) Shu, C.; Zhang, H.; Olankitwanit, A.; Rajca, S.; Rajca, A. High-Spin Diradical Dication of Chiral  $\pi$ -Conjugated Double Helical Molecule. *J. Am. Chem. Soc.* **2019**, *141* (43), 17287–17294.
- (21) Gallagher, N.; Zhang, H.; Junghoefer, T.; Giangrisostomi, E.; Ovsyannikov, R.; Pink, M.; Rajca, S.; Casu, M. B.; Rajca, A. Thermally and Magnetically Robust Triplet Ground State Diradical. *J. Am. Chem. Soc.* **2019**, *141*, 4764.
- (22) Ravat, P.; Solomek, T.; Häussinger, D.; Blacque, O.; Juríček, M. Dimethylcethrene: A Chiroptical Diradicaloid Photoswitch. *J. Am. Chem. Soc.* **2018**, *140* (34), 10839–10847.
- (23) Jiang, C.; Bang, Y.; Wang, X.; Lu, X.; Lim, Z.; Wei, H.; El-Hankari, S.; Wu, J.; Zeng, Z. Tetrabenzo-Chichibabin's Hydrocarbons: Substituent Effects and Unusual Thermochromic and Thermomagnetic Behaviours. *Chem. Commun.* **2018**, *54* (19), 2389–2392.
- (24) Kishi, R.; Murata, Y.; Saito, M.; Morita, K.; Abe, M.; Nakano, M. Theoretical Study on Diradical Characters and Nonlinear Optical Properties of 1,3-Diradical Compounds. *J. Phys. Chem. A* **2014**, *118* (45), 10837–10848.
- (25) Abe, M.; Kawanami, S.; Ishihara, C.; Nojima, M. 2-Silyl Group Effect on the Reactivity of Cyclopentane-1,3-Diyls. Intramolecular Ring-Closure versus Silyl Migration. *J. Org. Chem.* **2004**, *69* (17), 5622–5626.
- (26) Abe, M.; Kubo, E.; Nozaki, K.; Matsuo, T.; Hayashi, T. An Extremely Long-Lived Singlet 4,4-Dimethoxy-3,5-Diphenylpyrazoline-3,5-Diyl Derivative: A Notable Nitrogen-Atom Effect on Intra- and Intermolecular Reactivity. *Angew. Chem., Int. Ed.* **2006**, *45* (46), 7828–7831.
- (27) Yoshidomi, S.; Mishima, M.; Seyama, S.; Abe, M.; Fujiwara, Y.; Ishibashi, T.-A. Direct Detection of a Chemical Equilibrium between a Localized Singlet Diradical and Its  $\sigma$ -Bonded Species by Time-Resolved UV/Vis and IR Spectroscopy. *Angew. Chem., Int. Ed.* **2017**, *56* (11), 2984–2988.
- (28) Yoshidomi, S.; Abe, M. 1,2-Diazacyclopentane-3,5-Diyl Diradicals: Electronic Structure and Reactivity. *J. Am. Chem. Soc.* **2019**, *141* (9), 3920–3933.
- (29) Stuyver, T.; Chen, B.; Zeng, T.; Geerlings, P.; De Proft, F.; Hoffmann, R. Do Diradicals Behave Like Radicals? *Chem. Rev.* **2019**, *119* (21), 11291–11351.
- (30) Xu, J. D.; Hrovat, D. A.; Borden, W. T. Ab Initio Calculations of the Potential Surfaces for the Lowest Singlet and Triplet States of 2,2-Difluorocyclopentane-1,3-Diyl. The Singlet Diradical Lies Below the Triplet. *J. Am. Chem. Soc.* **1994**, *116* (6), 5425–5427.
- (31) Jasti, R.; Bhattacharjee, J.; Neaton, J. B.; Bertozzi, C. R. Synthesis, Characterization, and Theory of [9]-, [12]-, and [18]-Cycloparaphenylenes: Carbon Nano Hoop Structures. *J. Am. Chem. Soc.* **2008**, *130* (52), 17646–17647.
- (32) Takaba, H.; Omachi, H.; Yamamoto, Y.; Bouffard, J.; Itami, K. Selective Synthesis of [12]Cycloparaphenylenes. *Angew. Chem., Int. Ed.* **2009**, *48* (33), 6112–6116.
- (33) Yamago, S.; Watanabe, Y.; Iwamoto, T. Synthesis of [8]Cycloparaphenylenes from a Square-Shaped Tetranuclear Platinum Complex. *Angew. Chem., Int. Ed.* **2010**, *49* (4), 757–759.
- (34) Iwamoto, T.; Watanabe, Y.; Sakamoto, Y.; Suzuki, T.; Yamago, S. Selective and Random Syntheses of [n]Cycloparaphenylenes ( $n = 8–13$ ) and Size Dependence of Their Electronic Properties. *J. Am. Chem. Soc.* **2011**, *133* (21), 8354–8361.
- (35) Darzi, E. R.; Jasti, R. The Dynamic, Size-Dependent Properties of [5]-[12]Cycloparaphenylenes. *Chem. Soc. Rev.* **2015**, *44* (18), 6401–6410.
- (36) Li, Y.; Segawa, Y.; Yagi, A.; Itami, K. A Nonalternant Aromatic Belt: Methylene-Bridged [6]Cycloparaphenylenes Synthesized from Pillar[6]Arene. *J. Am. Chem. Soc.* **2020**, *142* (29), 12850–12856.
- (37) Matsumoto, M.; Antol, I.; Abe, M. Curve Effect on Singlet Diradical Contribution in Kekulé-Type Diradicals: A Sensitive Probe for Quinoidal Structure in Curved  $\pi$ -Conjugated Molecules. *Molecules* **2019**, *24* (1), 209.
- (38) Li, P.; Sisto, T. J.; Darzi, E. R.; Jasti, R. The Effects of Cyclic Conjugation and Bending on the Optoelectronic Properties of Paraphenylenes. *Org. Lett.* **2014**, *16* (1), 182–185.
- (39) Stratmann, R. E.; Scuseria, G. E.; Frisch, M. J. An Efficient Implementation of Time-Dependent Density-Functional Theory for the Calculation of Excitation Energies of Large Molecules. *J. Chem. Phys.* **1998**, *109* (19), 8218–8224.
- (40) Becke, A. D. Density-functional Thermochemistry. III. The Role of Exact Exchange. *J. Chem. Phys.* **1993**, *98* (7), 5648–5652.
- (41) Lee, C.; Yang, W.; Parr, R. G. Development of the Colic-Salvetti Correlation-Energy into a Functional of the Electron Density Formula Chengteh. *Phys. Rev. B: Condens. Matter Mater. Phys.* **1988**, *37*, 785–789.
- (42) Evans, P. J.; Darzi, E. R.; Jasti, R. Efficient Roomerature Synthesis of a Highly Strained Carbon Nanohoop Fragment of Buckminsterfullerene. *Nat. Chem.* **2014**, *6* (5), 404–408.
- (43) Kayahara, E.; Patel, V. K.; Yamago, S. Synthesis and Characterization of [5]Cycloparaphenylenes. *J. Am. Chem. Soc.* **2014**, *136* (6), 2284–2287.
- (44) Xia, J.; Jasti, R. Synthesis, Characterization, and Crystal Structure of [6]Cycloparaphenylenes. *Angew. Chem., Int. Ed.* **2012**, *51* (10), 2474–2476.
- (45) Lovell, T. C.; Colwell, C. E.; Zakharov, L. N.; Jasti, R. Symmetry Breaking and the Turn-on Fluorescence of Small, Highly Strained Carbon Nanohoops. *Chem. Sci.* **2019**, *10* (13), 3786–3790.
- (46) Suenobu, T.; Arahori, I.; Nakayama, K. I.; Suzuki, T.; Katoh, R.; Nakagawa, T. Reaction of Oxygen with the Singlet Excited State of [n]Cycloparaphenylenes ( $n = 9, 12$ , and  $15$ ): A Time-Resolved Transient Absorption Study Seamlessly Covering Time Ranges from Subnanoseconds to Microseconds by the Randomly-Interleaved-Pulse-Train Method. *J. Phys. Chem. A* **2020**, *124* (1), 46–55.
- (47) Tanaka, F.; Tsumura, K.; Furuta, T.; Iwamoto, K.; Okamoto, M. Efficiencies of Singlet Oxygen Production and Rate Constants for Oxygen Quenching in the S1 State of Dicyanonaphthalenes and Related Compounds. *Photochem. Photobiol. Sci.* **2008**, *7* (1), 56–62.
- (48) Nakagawa, T.; Okamoto, K.; Hanada, H.; Katoh, R. Probing with Randomly Interleaved Pulse Train Bridges the Gap between Ultrafast Pump-Probe and Nanosecond Flash Photolysis. *Opt. Lett.* **2016**, *41* (7), 1498–1501.
- (49) Adam, W.; Nau, W. M.; Fragale, G.; Wirz, J.; Klapstein, D. Phosphorescence and Transient Absorption of Azoalkane Triplet States. *J. Am. Chem. Soc.* **1995**, *117* (50), 12578–12592.
- (50) Eaton, S. S.; More, K. M.; Sawant, B. M.; Eaton, G. R. Use of the EPR Half-Field Transition To Determine the Interspin Distance and the Orientation of the Interspin Vector in Systems with Two Unpaired Electrons. *J. Am. Chem. Soc.* **1983**, *105* (22), 6560–6567.
- (51) Adam, W.; Kita, F.; Harrer, H. M.; Nau, W. M.; Zipf, R. The D Parameter (EPR Zero-Field Splitting) of Localized 1,3-Cyclopentanediyl Triplet Diradicals as a Measure of Electronic Substituent Effects on the Spin Densities in Para-Substituted Benzyl-Type Radicals. *J. Org. Chem.* **1996**, *61* (20), 7056–7065.
- (52) Adam, W.; Van Barneveld, C.; Emmert, O. The EPR D Parameter as a Measure of Spin Delocalization in Cyclopentane-1,3-Diyl Triplet Diradicals with Extended Conjugation  $\pi$ -Type Substituents. *J. Chem. Soc. Perkin Trans. 2* **2000**, No. 4, 637–641.
- (53) Sinnecker, S.; Neese, F. Spin-Spin Contributions to the Zero-Field Splitting Tensor in Organic Triplets, Carbenes and Biradicals - A Density Functional and Ab Initio Study. *J. Phys. Chem. A* **2006**, *110* (44), 12267–12275.
- (54) Neese, F. Calculation of the Zero-Field Splitting Tensor on the Basis of Hybrid Density Functional and Hartree-Fock Theory. *J. Chem. Phys.* **2007**, *127* (16), 164112.

- (55) Neese, F. The ORCA Program System. *Wiley Interdiscip. Rev.: Comput. Mol. Sci.* **2012**, *2* (1), 73–78.
- (56) Neese, F. Software Update: The ORCA Program System, Version 4.0. *Wiley Interdiscip. Rev.: Comput. Mol. Sci.* **2018**, *8* (1), 4–9.
- (57) Buchwalter, S. L.; Gloss, G. L. An Electron Spin Resonance Study of Matrix Isolated 1,3-Cyclopentadiyl, a Localized 1,3-Carbon Biradical. *J. Am. Chem. Soc.* **1975**, *97* (13), 3857–3858.
- (58) Wang, Z.; Akisaka, R.; Yabumoto, S.; Nakagawa, T.; Hatano, S.; Abe, M. Impact of the Macroyclic Structure and Dynamic Solvent Effect on the Reactivity of a Localised Singlet Diradicaloid with  $\pi$ -Single Bonding Character. *Chem. Sci.* **2021**, *12*, 613–625.
- (59) Adam, W.; Maas, W.; Nau, W. M. Wavelength-Selective Photodenitrogenation of Azoalkanes to High-Spin Polyradicals with Cyclopentane-1,3-Diyil Spin-Carrying Units and Their Photobleaching: EPR/UV Spectroscopy and Product Studies of the Matrix-Isolated Species. *J. Org. Chem.* **2000**, *65* (25), 8790–8796.
- (60) Bleaney, B.; Bowers, K.D. Anomalous Paramagnetism of Copper Acetate. *Proc. R. Soc. A* **1952**, *43*, 372–374.
- (61) Yanai, T.; Tew, D. P.; Handy, N. C. A New Hybrid Exchange-Correlation Functional Using the Coulomb-Attenuating Method (CAM-B3LYP). *Chem. Phys. Lett.* **2004**, *393* (1–3), 51–57.
- (62) Hegarty, D.; Robb, M. A. Application of Unitary Group Methods to Configuration Interaction Calculations. *Mol. Phys.* **1979**, *38* (6), 1795–1812.
- (63) Frisch, M. J.; Trucks, G. W.; Schlegel, H. B.; Scuseria, G. E.; Robb, M. A.; Cheeseman, J. R.; Scalmani, G.; Barone, V.; Petersson, G. A.; Nakatsuji, H.; Li, X.; Caricato, M.; Marenich, A. V.; Bloino, J.; Janesko, B. G.; Gomperts, R.; Mennucci, B.; Hratchian, H. P.; J., V., **2016**. No Title. 2016.
- (64) Yamaguchi, K.; Jensen, F.; Dorigo, A.; Houk, K. N. A Spin Correction Procedure for Unrestricted Hartree-Fock and Møller-Plesset Wavefunctions for Singlet Diradicals and Polyradicals. *Chem. Phys. Lett.* **1988**, *149* (5–6), 537–542.
- (65) Andersson, K. Different Forms of the Zeroth-Order Hamiltonian in Second-Order Perturbation Theory with a Complete Active Space Self-Consistent Field Reference Function. *Theor. Chim. Acta* **1995**, *91* (1–2), 31–46.
- (66) Hoffmann, R. Interaction of Orbitals through Space and through Bonds. *Acc. Chem. Res.* **1971**, *4* (1), 1–9.
- (67) Hoffmann, R. Trimethylene and the Addition of Methylene to Ethylene. *J. Am. Chem. Soc.* **1968**, *90* (6), 1475–1485.
- (68) Abe, M.; Ishihara, C.; Nojima, M. DFT Prediction of Ground-State Spin Multiplicity of Cyclobutane-1,3-Diyls: Notable Effects of Two Sets of through-Bond Interactions. *J. Org. Chem.* **2003**, *68* (4), 1618–1621.
- (69) Abe, M.; Ishihara, C.; Tagegami, A. Theoretical Calculations of the Effects of 2-Heavier Group 14 Element and Substituents on the Singlet-Triplet Energy Gap in Cyclopentane-1,3-Diyls and Computational Prediction of the Reactivity of Singlet 2-Silacyclopentane-1,3-Diyls. *J. Org. Chem.* **2004**, *69* (21), 7250–7255.
- (70) Borden, W. T. Effects of Electron Donation into C-F  $\Sigma^*$  Orbitals: Explanations, Predictions and Experimental Tests. *Chem. Commun.* **1998**, No. 18, 1919–1925.
- (71) <https://gitlab.com/Molcas/OpenMolcas>.
- (72) Nakagaki, T.; Sakai, T.; Mizuta, T.; Fujiwara, Y.; Abe, M. Kinetic Stabilization and Reactivity of  $\pi$  Single-Bonded Species: Effect of the Alkoxy Group on the Lifetime of Singlet 2,2-Dialkoxy-1,3-Diphenyloctahydronaphthalene-1,3-Diyls. *Chem. - Eur. J.* **2013**, *19* (31), 10395–10404.
- (73) Segawa, Y.; Omachi, H.; Itami, K. Theoretical Studies on the Structures and Strain Energies of Cycloparaphenylenes. *Org. Lett.* **2010**, *12* (10), 2262–2265.
- (74) Krygowski, T. M.; Cyrański, M. K. Structural Aspects of Aromaticity. *Chem. Rev.* **2001**, *101* (5), 1385–1419.
- (75) Rickhaus, M.; Jirasek, M.; Tejerina, L.; Gotfredsen, H.; Peeks, M. D.; Haver, R.; Jiang, H. W.; Claridge, T. D. W.; Anderson, H. L. Global Aromaticity at the Nanoscale. *Nat. Chem.* **2020**, *12* (3), 236–241.
- (76) Peeks, M. D.; Gong, J. Q.; McLoughlin, K.; Kobatake, T.; Haver, R.; Herz, L. M.; Anderson, H. L. Aromaticity and Antiaromaticity in the Excited States of Porphyrin Nanorings. *J. Phys. Chem. Lett.* **2019**, *10* (8), 2017–2022.
- (77) Schleyer, P. v. R.; Jiao, H.; Hommes, N. J. R. v. E.; Malkin, V. G.; Malkina, O. L. An Evaluation of the Aromaticity of Inorganic Rings: Refined Evidence from Magnetic Properties. *J. Am. Chem. Soc.* **1997**, *119* (51), 12669–12670.
- (78) Burley, G. A. Trannulenes with “in-Plane” Aromaticity: Candidates for Harvesting Light Energy. *Angew. Chem., Int. Ed.* **2005**, *44*, 3176–3178.
- (79) Toriumi, N.; Muranaka, A.; Kayahara, E.; Yamago, S.; Uchiyama, M. In-Plane Aromaticity in Cycloparaphenylenes Dications: A Magnetic Circular Dichroism and Theoretical Study. *J. Am. Chem. Soc.* **2015**, *137* (1), 82–85.
- (80) Williams, R. V. Homoaromaticity. *Chem. Rev.* **2001**, *101* (5), 1185–1204.
- (81) Winstein, S.; Sonnenberg, J.; Devries, L. Homo-Aromatic Structures. *J. Am. Chem. Soc.* **1959**, *81* (24), 6524–6525.
- (82) Schleyer, P. v. R.; Maerker, C.; Dransfeld, A.; Jiao, H.; van Eikema Hommes, N. J. R. Nucleus-Independent Chemical Shifts: A Simple and Efficient Aromaticity Probe. *J. Am. Chem. Soc.* **1996**, *118* (26), 6317–6318.
- (83) Steiner, E.; Fowler, P. W.; Jenneskens, L. W. Counter-Rotating Ring Currents in Coronene and Corannulene. *Angew. Chem., Int. Ed.* **2001**, *40* (2), 362–366.
- (84) Fallah-Bagher-Shaiedai, H.; Wannere, C. S.; Corminboeuf, C.; Puchta, R.; Schleyer, P. V. R. Which NICS Aromaticity Index for Planar  $\pi$  Rings Is Best? *Org. Lett.* **2006**, *8* (5), 863–866.
- (85) Geuenich, D.; Hess, K.; Köhler, F.; Herges, R. Anisotropy of the Induced Current Density (ACID), a General Method to Quantify and Visualize Electronic Delocalization. *Chem. Rev.* **2005**, *105* (10), 3758–3772.